REVIEW

National Science Review
8: nwab104, 2021
https://doi.org/10.1093/nsr/nwab104
Advance access publication 12 June 2021

[1]Eco-Materials and Renewable Energy Research Center (ERERC), Jiangsu Key Laboratory for Nano Technology, National Laboratory of Solid State Microstructures, School of Physics, Nanjing University, Nanjing 210093, China; [2]Qian Xuesen Laboratory of Space Technology, China Academy of Space Technology, Beijing 100094, China; [3]Collaborative Innovation Center of Advanced Microstructures, College of Engineering and Applied Sciences, Nanjing University, Nanjing 210093, China; [4]Kunshan Innovation Institute of Nanjing University, Suzhou 215347, China; [5]School of Science and Engineering, The Chinese University of Hong Kong, Shenzhen 518172, China; [6]Macau Institute of Systems Engineering, Macau University of Science and Technology, Macau 999078, China and [7]Wuhan National Laboratory for Optoelectronics, Huazhong University of Science and Technology, Wuhan 430074, China

***Corresponding authors.** E-mails: yaoyingfang@nju.edu.cn; yaowei@qxslab.cn; zgzou@nju.edu.cn
†Equally contributed to this work.

Received 31 December 2020; **Revised** 28 May 2021; **Accepted** 10 June 2021

MATERIALS SCIENCE

Special Topic: Advanced Materials for Solar Energy Conversion

Extraterrestrial artificial photosynthetic materials for *in-situ* resource utilization

Liuqing Yang[1,†], Ce Zhang[2,†], Xiwen Yu[1,3,†], Yingfang Yao[1,3,4,5,7,*], Zhaosheng Li[1,3], Congping Wu[1,4], Wei Yao[2,*] and Zhigang Zou[1,2,3,5,6,*]

ABSTRACT

Aerospace milestones in human history, including returning to the moon and manned Martian missions, have been implemented in recent years. Space exploration has become one of the global common goals, and to ensure the survival and development of human beings in the extraterrestrial extreme environment has been becoming the basic ability and technology of manned space exploration. For the purpose of fulfilling the goal of extraterrestrial survival, researchers in Nanjing University and the China Academy of Space Technology proposed extraterrestrial artificial photosynthesis (EAP) technology. By simulating the natural photosynthesis of green plants on the Earth, EAP converts CO_2/H_2O into fuel and O_2 in an *in-situ*, accelerated and controllable manner by using waste CO_2 in the confined space of spacecraft, or abundant CO_2 resources in extraterrestrial celestial environments, e.g. Mars. Thus, the material loading of manned spacecraft can be greatly reduced to support affordable and sustainable deep space exploration. In this paper, EAP technology is compared with existing methods of converting CO_2/H_2O into fuel and O_2 in the aerospace field, especially the Sabatier method and Bosch reduction method. The research progress of possible EAP materials for *in-situ* utilization of extraterrestrial resources are also discussed in depth. Finally, this review lists the challenges that the EAP process may encounter, which need to be focused on for future implementation and application. We expect to deepen the understanding of artificial photosynthetic materials and technologies, and aim to strongly support the development of manned spaceflight.

Keywords: solar energy, extraterrestrial survival, artificial photosynthesis, CO_2 reduction, oxygen evolution

INTRODUCTION

Extraterrestrial survival is a prerequisite for humankind to achieve long-term space flight, extraterrestrial residence and immigration, and creates one of the greatest scientific and technological challenges of human deep space exploration. During human extraterrestrial exploration activities, a sustained supply of O_2 and fuel is one of the essential abilities. Extraterrestrial artificial photosynthesis (EAP), i.e. CO_2/H_2O conversion into fuel and O_2 from human respiration, combustion emissions and *in-situ* resources on outer-Earth planets, can greatly reduce the supply load of spacecraft and space stations, thus promoting affordable and sustainable human deep space exploration.

EAP (Fig. 1a) is a simulation of plant photosynthesis on Earth. Through photocatalysis [1,2] (Fig. 1b), photoelectrocatalysis [3,4] (Fig. 1c and d) or photovoltaic electrocatalysis [5] (Fig. 1e), EAP uses a controllable and accelerated chemical process to *in-situ* convert CO_2/H_2O into carbon-containing fuel and O_2 by harnessing solar radiation. Compared with traditional CO_2/H_2O conversion techniques, such as the thermochemical or electrochemical method, EAP technology, which only uses solar energy and semiconductor materials, is usually carried out without consuming auxiliary energy inputs. EAP can be applied to *in-situ* convert CO_2 waste in a confined space, which effectively reduces the supply demand of human space stations and deep

space spacecraft, etc. Furthermore, it also makes use of abundant *in-situ* resources such as CO_2 and H_2O in the extraterrestrial atmospheric environments of the moon or Mars to meet the material demand. Through EAP, human beings can survive in extraterrestrial environments in the long term.

In recent decades, for solving the key problems of supply demand for human space stations and deep space exploration, the USA, Japan and other countries have continuously carried out research on CO_2 conversion technology as one of the crucial parts of *in-situ* resource utilization, developed a series of CO_2 conversion systems based on the Sabatier method [6] and Bosch reduction method [7], and carried out experimental verification of CO_2 reduction and O_2 production on the International Space Station (ISS) [8,9]. In 2005, the National Aeronautics and Space Administration (NASA) in the USA proposed the Resource Prospector mission, planning to carry out *in-situ* utilization experiments for producing O_2 from water in lunar surface soil in 2022. Russia raised a series of plans for lunar exploration and will launch a lander named Moon 27 in 2025 for *in-situ* lunar resource utilization. However, existing CO_2 conversion devices adopting high-temperature and high-pressure reaction conditions always have high energy consumption. On the other hand, the extraterrestrial microgravity environment obviously promotes the formation of supersaturated layers of dissolved gas molecules near the electrode surface. These layers accelerate the formation and evolution of bubbles at the interface between electrode and electrolyte, and hinder the material transport rate at the microscopic scale [10–12]. The electrode reaction kinetics are thus significantly reduced, resulting in less than one-third of the working efficiency on the Earth. Furthermore, due to the lack of experimental data and related theoretical research, key scientific and technical challenges, such as *in-situ* preparation of photoelectrocatalytic materials, the heterogeneous catalytic process and the working parameters of materials and systems, have become major problems in CO_2 conversion.

The ability to harvest light energy through artificial photosynthesis may create an essential foundation for technologies used in many areas, such as global carbon neutralization [13]. Thus, it is reasonable to expect the further development of EAP for human extraterrestrial survival. With regard to this, one example is demonstrated by an EAP device, developed by Qian Xuesen Laboratory of Space Technology, which reduces CO_2 with water into a carbonaceous compound and produces O_2. The feasibility of the reactor in CO_2/H_2O photo-conversion into carbonaceous compound and O_2 was verified by ground experiment, which may provide a theoretical and practical foundation for subsequent device optimization, carbon dioxide conversion into variable hydrocarbon products with high selectivity, and in-orbit testing of artificial photosynthesis devices [14].

The research into artificial photosynthesis began in 1972 when Honda and Fujishima reported that H_2 was produced by photolysis of water over titanium dioxide electrodes under ultraviolet light [4]. Then during the following few decades, numerous scientists carried out a series of research works on this specific area. In 2001, Zhigang Zou proposed a new theory and method to regulate the band structure of photocatalytic materials, and broadened the response range of photocatalytic materials. He realized visible-light-induced complete water decomposition [2] and CO_2 reduction [15] under visible light, thus developing a new-generation visible-light-responsive photocatalytic material. In 2015, NASA started to focus on artificial photosynthesis and proposed the concept of microbial-assisted artificial photosynthesis. In 2016, Daniel G. Nocera devised a biocompatible-inorganic catalyst system to decompose water to get H_2 and O_2 at low voltages [16] (Fig. 1f). He utilized low concentrations of CO_2 in the presence of O_2 and H_2 to generate biomass, fuel or chemical products. A 10% energy efficiency of CO_2 reduction could be obtained when coupling this device with a photovoltaic system. Peidong Yang combined light-absorbing semiconductor nanomaterials with bacteria to produce biological-inorganic hybrid systems for CO_2 fixation [17,18] (Fig. 1g and h). In 2017, Nanjing University and Qian Xuesen Laboratory at the China Academy of Space Technology carried out research into EAP materials and systems for the first time, aiming to resolve the requirements with regard to basic materials and energy during human extraterrestrial survival, and they have preliminarily completed the verification of materials and systems. This research progress provides the technical foundation for human survival during spaceflight missions and deep space exploration.

EXTRATERRESTRIAL ENVIRONMENTAL IMPACT

Space exploration activities are faced with various special environments, such as microgravity, strong radiation, extreme temperature and high vacuum, which bring about a series of challenges for realizing CO_2/H_2O conversion in outer space. Only through long-term and effective experiments, combined with ground simulation and in-orbit verification, can we investigate the mechanistic and process influences of outer space on EAP in the process of space exploration. However, it can be speculated that the

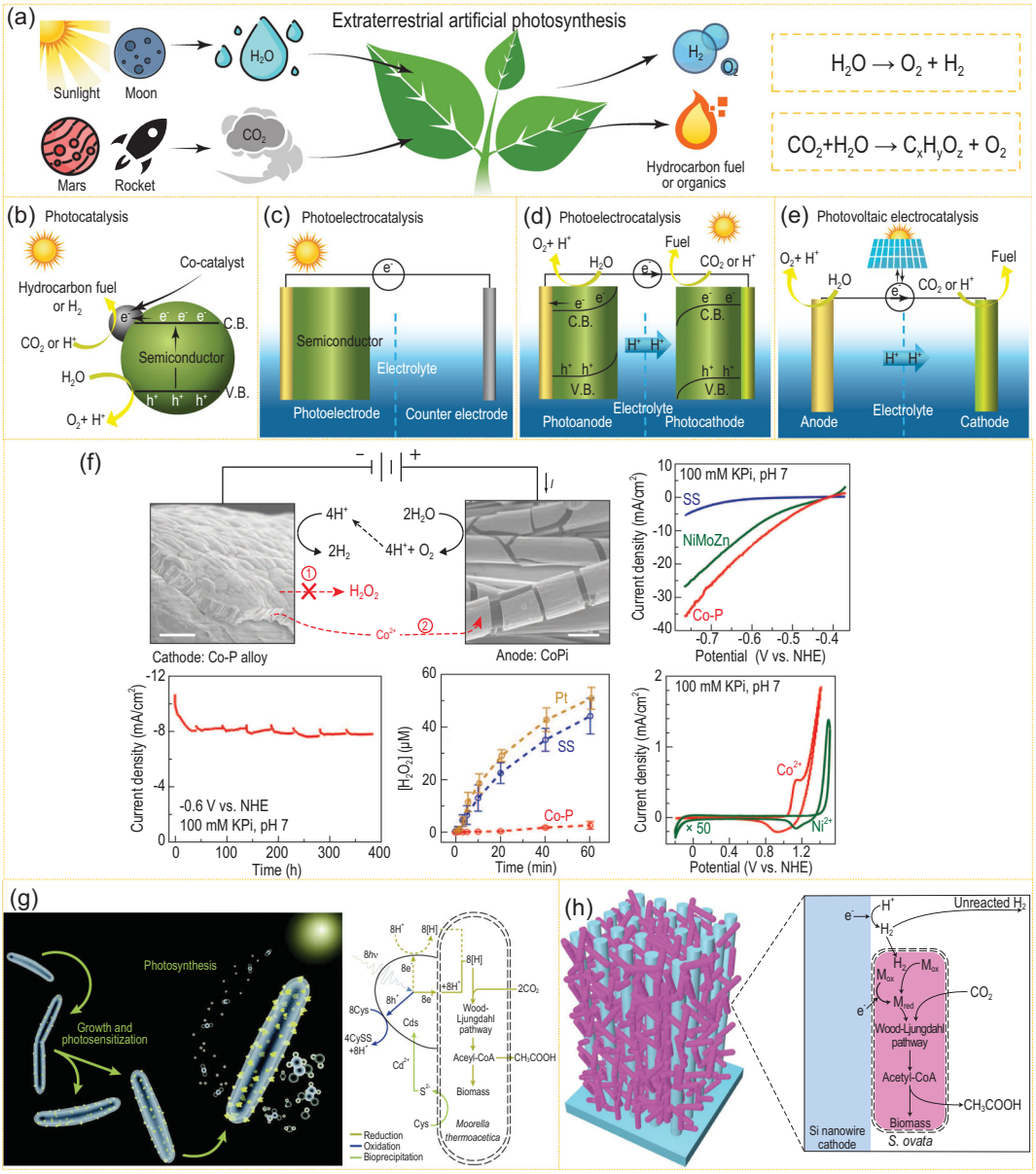

Figure 1. Mechanism schemes of (a) EAP, (b) photocatalysis, (c and d) photoelectrocatalysis and (e) photovoltaic electrocatalysis. (f) A biocompatible inorganic water-splitting catalyst system (adapted from ref. [16] with permission from American Association for the Advancement of Science (AAAS)). (g) Scheme of CO_2 reduction of the bacteria/semiconductor hybrid artificial photosynthetic system (adapted from ref. [17] with permission from AAAS). (h) Illustrations of a nanowire-bacteria hybrid system and the reaction mechanism (adapted from ref. [18] with permission from Elsevier).

external factors that mainly affect CO_2 and H_2O conversion may be, and are not limited to, the following aspects:

(i) Microgravity. Under microgravity, the key problems of bubble formation, evolution and detachment at the reaction interface need to be solved urgently.

(ii) Cosmic radiation. Materials, especially semiconductors, on the lunar surface or in Earth orbit would be strongly affected by the impact of rays or particles such as electrons, protons, heavy ions and plasma. Material properties will be changed by electromagnetic radiation and charged particles, including X-rays, electrons, protons and heavy ions, mainly due to the internal interactions in materials during the bombardment caused by cosmic rays or high energy particles. These internal interactions are divided into coulomb interactions and electromagnetic effects.

Coulomb interactions include three cases: Coulomb scattering, bremsstrahlung and inelastic collision between particles and electrons. Coulomb scattering refers to the elastic collision process in which charged particles are incident to matter, then deflected and dispersed by the Coulomb electric field force of the atomic nucleus. When materials are incident by high-energy electrons, the high-speed electron suddenly slows down and produces the bremsstrahlung, which is an important process for charged particles to act on materials in space. When particles or electrons inelastically collide with material, the electron in the material is ionized or excited from the outer layer to the inner layer, causing primary ionization to produce a large number of secondary electrons. The total kinetic energy before and after collision is not equal.

Electromagnetic interaction mainly refers to the interaction between high-energy rays and materials. The whole, or part, of the initial energy of the high-energy ray can be transferred to electrons in the materials, and the incident particles disappear or scatter. Electromagnetic effects include the photoelectric effect, electron pair effect and Compton effect. The dominant effect of electromagnetic action is related to photon energy and atomic coefficient of absorbing material.

After the incident particles enter the material, the energy of the incident particles decreases and the velocity slows down. Finally, the incident particles are blocked or scattered. The charged particles enter the material and lose energy through two ways: the displacement effect and ionization effect. The displacement effect is when charged particles collide with the nucleus, making atoms leave their original positions; or the incident particles fill in the lattice gaps to form vacancies and interstitial atoms, leading to the corresponding changes in material structure and properties. Collision between incident high-energy particles and material atoms is the main source of energy loss. Further, a large number of recoil atoms are produced after collision, and the secondary reactions of recoil atoms with the surrounding atoms form a large number of Frenkel defects. Most of these defects are semi-permanent, leading to great damage to semiconductor materials and devices. The ionization effect is when the radiation of charged particles with a certain energy excites electrons outside the nucleus of materials to form free electrons. Material atoms thus become positive ions, forming electron-hole pairs. When electrons transition from valence band to conduction band, the electrical, chemical, physical and mechanical properties of materials can be affected. Small-dose and long-term steady-state radiation in space often leads to a cumulative ionization damage effect.

(iii) Extreme temperature. Extraterrestrial space, including the lunar surface, produces a huge temperature difference between day and night. During daytime, when the sun shines vertically, the temperature rises as high as 127°C; at night, the temperature can be as low as −183°C. As water evaporates or freezes easily, this poses a great challenge to CO_2 reduction in aqueous systems. Furthermore, the thermal expansion and contraction caused by temperature switching generally accelerates the fatigue and aging of materials, which brings a series of system durability and reliability problems.

In addition, there are other problems caused by the atmospheric pressure and special atmospheric environments of extraterrestrial planets, although some of them, e.g. extreme temperatures and ultra-vacuums, can be resolved by aerospace engineering methods. For example, the Environmental Control and Life Support System (ECLSS) used on the ISS by NASA can maintain the space capsule pressure, temperature and humidity. Extreme conditions have brought great challenges for researchers in selecting and designing materials, and it will also become difficulties in our research of extraterrestrial artificial photosynthsis.

RECENT PROGRESS ON EXTRATERRESTRIAL CO_2 AND H_2O CONVERSION FOR SPACECRAFT

Since the 1960s, the Sabatier method [6] and Bosch reduction method [7] have been the main approaches in CO_2 reduction technology. H_2O electrolysis for H_2 and O_2 has also been widely anticipated [19]. Recently, the EAP technology proposed by Nanjing University and Qian Xuesen Laboratory realized CO_2/H_2O photo-conversion under mild conditions with low energy consumption (Fig. 2a and b).

For solving the key problems of manned space stations and deep space exploration, the USA and other countries carried out research on CO_2 and H_2O conversion based on traditional ground technology, e.g. by using H_2O electrolysis to supply

O_2 for astronauts in the ISS. To realize the recycling of CO_2 released by astronauts, NASA and Japan Aerospace Exploration Agency (JAXA) have developed a set of CO_2 reduction and O_2 evolution devices, in which CO_2 reduction is obtained by converting CO_2 and H_2 into methane with H_2 obtained by H_2O electrolysis. The Sabatier reactor contains a gas-solid two-phase process with a core unit temperature of 250–450°C and a minimum gas pressure of 55 kPa. The mass of the ground experimental unit is around 41 kg and the total power is >100 W. The in-orbit test was completed for this system in October 2010 (Fig. 2c and d) [6,20]. The water electrolyzer developed by JAXA has also been tested in orbit [8,9]. This device was obtained by modifying the more technically mature proton exchange membrane electrolytic cell, which consists of an electrolytic unit and a gas-liquid separation unit [9,21] (Fig. 2e and f). In the ISS, a combination of the above two devices was tested to support the ECLSS to convert CO_2 into O_2 and methane by in-orbit reaction (Fig. 2g) [9]. JAXA researchers used parabolic flight and drop tower tests to make a series of research and improvement works on the water electrolysis device, including tests on the working temperature of the electrolytic cells, the pressure of the gas-liquid separation membranes, the electrolyte component, and the working voltage and current. However, even after various optimizations, the water electrolytic device's efficiency under microgravity was less than a third of that under usual gravity environments. The supersaturated layers of dissolved gas molecules formed by the aggregation of over-dissolved gas on the electrode highly hindered the transport rate and reaction efficiency of electrolyte [10] (Fig. 2h and i). Matsushima *et al.* found that the interaction between electrodes and electrolytes in the microgravity environment has a significant impact on the formation and evolution of bubbles, and the electrolytic performance [12]. In order to improve the material transport rate and reaction efficiency under microgravity, Nanjing University and Qian Xuesen Laboratory used liquid shearing force to compel the generated gas from the electrode surface, to prevent bubble gathering near the electrode surface under microgravity conditions [14].

For the more challenging manned deep space exploration missions, the USA first proposed the scheme of producing O_2 and fuel by using *in-situ* resources such as water and carbon dioxide on the moon or Mars. NASA proposed a Mars *in-situ*-propellant-production precursor (MIP) plan in 2001 to deoxidize carbon dioxide into O_2 using high-temperature electrolysis (Fig. 2j) [22]. In 2013, NASA also proposed a Mars *in-situ* resource utilization landing mission, MARCO POLO [23], which would utilize Mars's atmospheric and soil resources to produce H_2, O_2 and CH_4 by the Sabatier method and water electrolytic technology. They further proposed the Mars Oxygen ISRU Experiment (MOXIE) load in 2014 to deoxidize carbon dioxide in the Martian atmosphere to generate O_2 with a solid oxide electrolytic cell at 800°C to achieve 10 g h^{-1} O_2 production (Fig. 2k) [24]. The load project was launched in 2020, with about 2 h of experiments on Mars. If this *in-situ* resource utilization technology is validated, NASA will plan to follow up with a 100-fold magnificated scale device to support the 2033 manned Mars mission. In 2018, NASA supported a plan named the CO_2 Conversion Challenge to develop novel synthesis technologies that use carbon dioxide to generate molecules that can be used to manufacture a variety of products. However, the selected projects have remained at the laboratory stage and do not show feasibility for application to spacecraft. The USA is extracting O_2 from the Martian atmosphere as part of the 'Mars 2020' rover project (Fig. 2l) [24]. Generally, the American space mission in CO_2 utilization and transformation mainly uses the relatively mature thermal or electrical chemical conversion technology found in industry. Although the technical route has high maturity and stability, it needs to be carried out under extremely high temperature conditions (900–1600°C), with harsh operating conditions and large energy consumption, which is not conducive to manned deep space exploration. In 2020, Qian Xuesen Laboratory developed a demo of an EAP device for reducing carbon dioxide with water into carbonaceous compound and producing O_2 [14]. The feasibility of the reactor in reducing carbon dioxide to O_2 and carbonaceous compound was verified by ground experiment, which may provide a theoretical and practical foundation for subsequent device optimization, carbon dioxide conversion to variable hydrocarbon products with high selectivity, and on-orbit testing of artificial photosynthesis devices.

MATERIALS FOR EAP

Even on the moon or Mars, the energy provided by the sun is considerable. The light intensity on the moon approximates 1.4 times that of the Earth. Recent research shows that the permanent light area on the moon is adjacent to the ice area, which may be an ideal place for human beings to set up bases on the moon [25]. Solar power on Mars's surface is nearly 40% of that found on Earth. Because there is no atmospheric absorption, the solar spectrum on the surface of the moon is similar to that in Earth orbit, which is about equal to AM0

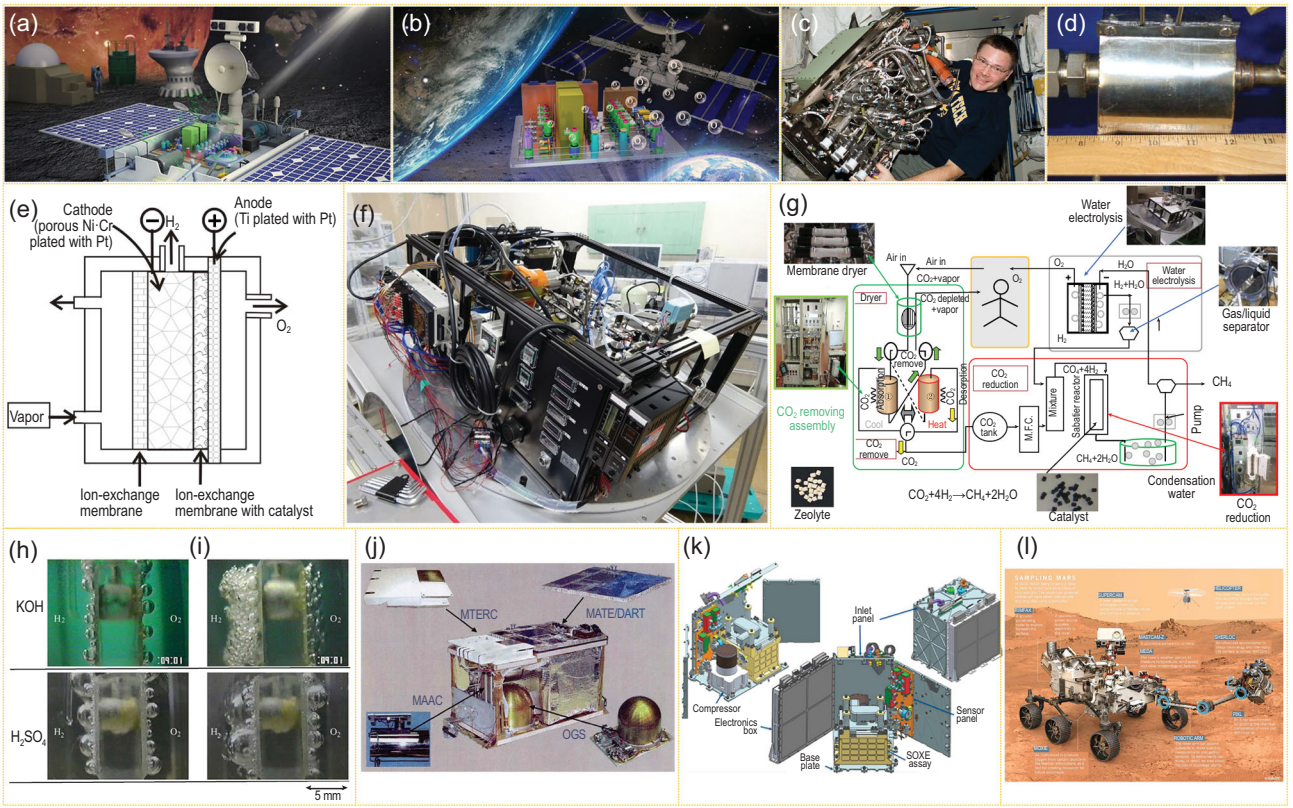

Figure 2. (a) Space exploration experiment device using *in-situ* resources to produce O_2. (b) Partial enlargement of (a). (c) Sabatier reaction system loaded into the ISS (adapted from ref. [6] with permission from American Institute of Aeronautics and Astronautics (AAIA)). (d) The core unit of the reactor (adapted from ref. [20] with permission from AIAA). (e) The principle of the reactor (adapted from ref. [21] with permission from AIAA) and (f) exterior feature of the JAXA water electrolyzer (adapted from ref. [9] with permission from AIAA). (g) New conceptual ECLSS in space station (adapted from ref. [9] with permission from AIAA). (h) Comparison of electrode in the environments of normal gravity on Earth (adapted from ref. [10] with permission from Elsevier). (i) Microgravity in space during the water electrolyzing process (adapted from ref. [11] with permission from Elsevier). (j) MIP CO_2 converting system (adapted from ref. [22] with permission from AIAA). (k) MOXIE CO_2 converting system (adapted from ref. [24] with permission from Elsevier). (l) Set-up diagram of 'Mars 2020' (adapted from ref. [24] with permission from Elsevier).

(1366.1 $W\,m^{-2}$). The transmitted sunlight wavelength on the surface of Mars increases with the increase of solar zenith angle and optical depth, and the energy at shorter wavelengths is more easily exhausted, because the cross section of dust particles suspended in the atmosphere at shorter wavelengths is larger. The 60-degree spectrum of sunlight on the surface of Mars is reduced to one-sixth of AM0, and further reduced in the blue part of the spectrum [26]. The moon has no atmosphere, thus there is no CO_2 on the moon. It is conservatively estimated that 0.3% to 1% of the water on the moon is buried in the form of ice under 40 cm of dry regolith [27]. On Mars, 95% of the atmosphere (the average pressure is <1% of one atmosphere) is CO_2. It has been estimated that Martian meteorites contain carbonates in low abundances (<1 vol.%) [28], and calcium carbonate has been identified in the soils at the Mars Phoenix landing site [29]. Thus, it is important to evaluate the feasibility of utilizing such mineralized carbon in future research. At this stage this review mainly focuses on the EAP process of CO_2/H_2O. Moreover, ground ice and hydration water exist at the near-surface subsurface of Mars [27]. The above preconditions are propitious to EAP in extraterrestrial environments such as the moon and Mars.

Most of the practical applications of EAP are based on photocatalytic materials. Photocatalysts are an important component to support artificial photosynthesis. Catalysts suitable for EAP are herein classified as photocatalysts, photoanodes, photocathodes and photovoltaic-electrochemical catalysts. The evaluation parameters for the performance assessment of the above catalysts mainly contain product rate, catalytic current density (for photoelectrocatalysts), turnover number and turnover frequency (evaluating the activity of catalytic active sites), quantum yield (assessing the performance of photocatalysts) and faradaic efficiency (assessing the selectivity for photoelectrocatalysts). In the

following text, we will mainly analyze photocatalytic/photoelectrocatalytic materials for EAP.

EAP processes mainly involve the conversion of CO_2 and H_2O into hydrocarbon fuel and O_2, and water splitting to produce H_2 and O_2. CO_2/H_2O photo-conversion involves two parts of the half reaction, including CO_2 reduction by photo-generated electrons, and H_2O oxidation by photo-generated holes, respectively. The standard chemical potentials required in thermodynamics for these processes are shown in the following reactions (1–8), respectively:

$$2H_2O + 2e^- \rightarrow H_2 \quad (E = 0\,V \text{ vs. SHE}), \tag{1}$$

$$2H_2O + 4h^+ \rightarrow 4H^+ + O_2 \quad (E = +1.23\,V \text{ vs. SHE}), \tag{2}$$

$$CO_2 + e^- \rightarrow CO_2{\cdot}^- \quad (E = -1.90\,V \text{ vs. SHE}), \tag{3}$$

$$CO_2 + 2H^+ + 2e^- \rightarrow CO + H_2O \quad (E = -0.53\,V \text{ vs. SHE}), \tag{4}$$

$$CO_2 + 2H^+ + 2e^- \rightarrow HCOOH \quad (E = -0.61\,V \text{ vs. SHE}), \tag{5}$$

$$CO_2 + 4H^+ + 4e^- \rightarrow HCHO + H_2O \quad (E = -0.48\,V \text{ vs. SHE}), \tag{6}$$

$$CO_2 + 6H^+ + 6e^- \rightarrow CH_3OH + H_2O \quad (E = -0.38\,V \text{ vs. SHE}), \tag{7}$$

$$CO_2 + 8H^+ + 8e^- \rightarrow CH_4 + 2H_2O \quad (E = -0.24\,V \text{ vs. SHE}). \tag{8}$$

In consideration of the extreme environmental conditions that EAP materials would be applied in, EAP materials should meet the following requirements: (i) an appropriate band structure, which is conducive for extraterrestrial sunlight absorption with different spectra and higher intensity, and reaches the chemical potentials needed to achieve the corresponding photo-redox reaction; (ii) adequate surface catalytic active sites to support effective photo-redox reaction; (iii) fast carrier transport and separation at the interface; (iv) stable activity under microgravity; (v) excellent survivability under intense cosmic radiations; (vi) great capability of resisting impact during take-off and landing; (vii) low cost. Additionally, CO_2/H_2O photocatalysts require excellence in reactant adsorption, product desorption and product selectivity. During CO_2/H_2O photo-conversion, H_2 production is the major competitive side reaction. Therefore, avoiding H_2 production is also one of the key points in improving CO_2/H_2O photo-conversion. A major way to hinder the H_2 production is to adjust the surface adsorption behavior of protons during the EAP process. Typical methods [30] include adjusting adsorption properties of the catalyst surface on carbon intermediate species, realizing proper surface modification and hydrating or alloying the surface with cocatalysts.

EAP materials for overall photo-conversion

Most of the reported photocatalytic materials are thermodynamically unfavorable to complete both the reductive half reaction (CO_2 reduction) and the oxidative half reaction (O_2 production), since the overall CO_2 conversion reaction generally needs a band gap of over 3.1 eV when taking account of the CO_2 adsorption on the electrode surface (reaction (3)). Catalysts with suitable band structure supporting overall CO_2/H_2O conversion are mainly TiO_2, ZnO, CdS, ZnS, $ZnIn_2S_4$, Ta_3N_5, TaON, graphitic carbon nitride (*g*-C_3N_4), $SrTiO_3$ [31–35] (in which TiO_2, ZnO and ZnS can only use ultraviolet light). $SrTiO_3$ and CdS can theoretically carry out full conversion under visible light, however, their intrinsic properties are restricted by low carrier separation rate. Thus, modification by cocatalysts or construction of composite materials is needed for the practical application of overall CO_2/H_2O conversion. Most of the cocatalysts in photocatalysis are derived from electrocatalysts. The role of cocatalysts is to reduce the activation energy required for surface reactions. Cocatalysts for oxygen evolution reaction (OER) mainly include cobalt phosphate (CoPi) [36], iron hydroxide oxide (FeOOH) [37], nickel oxide (NiO_x) [38], ceria (CeO_x) [39], RuO_2 [40], cobalt oxide (CoO_x) [41] and manganese oxide (MnO_x) [42]. Highly active cocatalysts for CO_2 reduction reaction (CO_2RR) primarily contain Au [43], Ag [44], Cu [45], Mn [46], MoS_2 [47] and CdS [48]. Moreover, adjusting the composition and ratio of metals, metallic alloy or other composite cocatalysts can be helpful in improving the selectivity of CO_2 reduction products [49–51].

At present, EAP materials are restricted by the low efficiency of photo-generated charge separation, the slow surface reaction rate and the serious inverse reaction of the products. A variety of

methods have been developed to regulate the charge separation and surface reaction performance, as well as restrain the inverse reaction of the artificial photosynthetic catalysts, including crystal engineering, built-in electric field, polarization effect, effective mass reduction of photo-generated carriers, a single crystal with low structural defects, molecular composites, the Z-scheme strategy and surface modification with cocatalysts. Conformation of solid solution is one of the effective means of regulating the electronic structure of catalysts and promoting photosynthetic performance. Zhigang Zou's group showed in their theoretical calculation results that Zn_2GeO_4 phase transformation from pseudo-cubic phase into cubic phase can effectively narrow the band gap. This is because the introduction of s and p orbitals of Ge enhances the repulsion of p-d (O 2p-Zn 3d) and raises the valence band position, while the s orbitals of Ge with low energy effectively lower the conduction band position. The solid solution photocatalysts composed of cubic $ZnGa_2O_4$ and pseudo-cubic Zn_2GeO_4 have light hole effective mass, and higher hole mobility. A narrow band gap is beneficial for absorbing sunlight with a wider wavelength, and high hole mobility is beneficial for improving the reaction rate of water oxidation. Therefore, the solid solution photocatalytic materials show higher photocatalytic performance with regard to reducing CO_2 to hydrocarbon fuel [52]. Based on a similar mechanism, Kazunari Domen's group also reported that ($Ga_{1-x}Zn_xN_{1-x}O_x$) has excellent performance for visible-light-driven complete water splitting [53].

It is an effective method to separate photo-generated charges by forming a built-in electric field on the interface of materials. Commonly, the built-in electric field exists between two different semiconductor materials or between different phase structures of the same semiconductor. The electrons and holes in this type of built-in electric field separate to opposite directions under the electric field, thus improving the separation efficiency. Zhigang Zou *et al.* synthesized a CeO_2 octahedral structure with vertical growth of hexahedron prism [54] (Fig. 3a). By adjusting the length and number of CeO_2 prisms with exposed surface of {1 0 0} facets on octahedron with surface of {1 1 1} facets, the separation and transmission efficiency of photo-generated carriers were improved, leading to the highly improved efficiency of photocatalytic CO_2 reduction to produce CH_4. Theoretical calculation showed that for CeO_2, the effective mass of electrons on {1 0 0} facet is much larger than that on {1 1 1} facet, while the effective mass of holes on {1 1 1} facet is larger than that on {1 0 0} facet. Therefore, photo-generated electrons easily migrate to the {1 1 1} facets, while photo-generated holes easily migrate to the {1 0 0} facets, which is conducive to the separation of photo-generated e^- and h^+. Thus, the CeO_2 homojunction materials achieved the overall CO_2/H_2O photo-conversion efficiency with 0.86 μmol h^{-1} g^{-1} CH_4 yield, and 0.2% quantum yield at 380 nm. The O_2 yield was also detected in accord with ~2 : 1 molar ratio to CH_4.

Polar semiconductors with asymmetric positive and negative electron centers can induce the polarization effect for effective separation of photo-generated charges. Zhigang Zou *et al.* proposed that single crystals growing along the polarization axis of a polar semiconductor could maximize the polarization field effect of the polar semiconductor, and efficiently separate photo-generated charges [55]. Because of the periodic potential field, the photo-generated charges are separated effectively along the polarization axis. And the photo-generated electrons are transmitted preferentially along the direction perpendicular to the polarization axis, forming a specific two-dimensional transport path, which greatly reduced the e^-–h^+ recombination probability. Thus, the activity and selectivity of reducing CO_2 to CH_4 are greatly improved. Li's group also found that the surface electric field induced by intrinsic polarity of GaN nanoarrays can effectively enhance carriers' spatial separation and greatly promote the photocatalytic overall water splitting. Based on the photo-generated charge separation effect between polar and non-polar surfaces, the quantum efficiency was improved from 0.9% to 6.9% with the redox cocatalysts constructed on polar and non-polar surfaces, respectively [56].

Carbon dots synthesized by microwave can quickly extract holes from carbon nitride and prevent the surface adsorption of methanol, which is beneficial to water oxidation and improves the ability of selective CO_2 reduction to alcohols. Tang and Guo's group found that the carbon dots synthesized by microwave method have unique hole-accepting properties, which can extend the electron lifetime of carbon nitride 6-fold [57]. It is thus beneficial to the stable production of stoichiometric O_2 and methanol from water and CO_2, respectively. The selectivity of CH_3OH is close to 100% and the inherent quantum efficiency is 2.1% under visible light. This work paves the way for the sustainable production of metal-free catalytic methanol, providing a unique strategy that can efficiently and selectively reduce CO_2 to high-value chemicals via artificial synthesis.

Nanostructured single-crystal photocatalysts with few structural defects and the appropriate cocatalysts were shown to be excellent in overall solar water splitting. For example, although Ta_3N_5

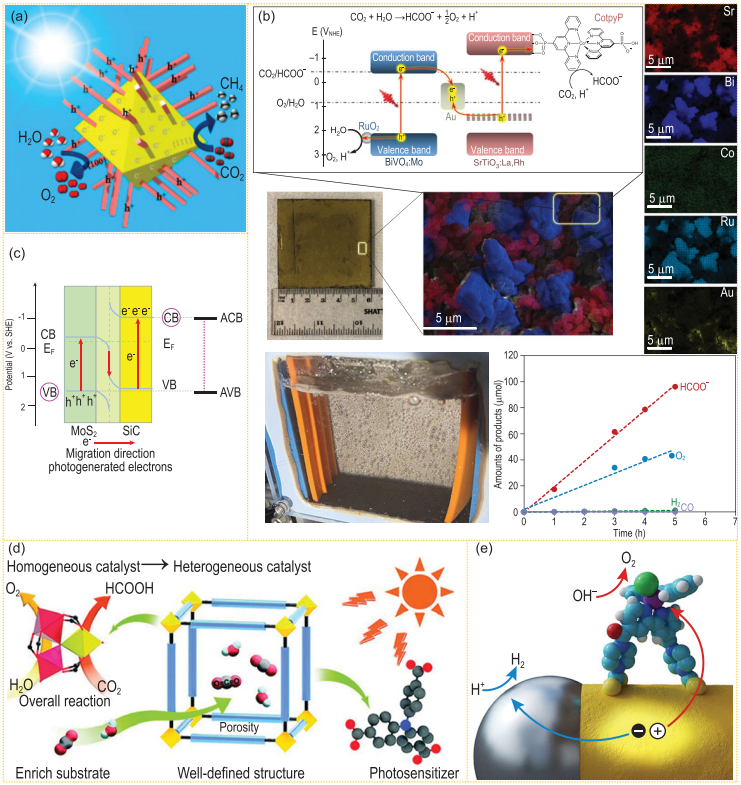

Figure 3. (a) Schematic illustration of CO_2 photoreduction into CH_4 over hexahedron prism anchored octahedronal CeO_2 (adapted from ref. [54] with permission from ACS Publications). (b) An overall CO_2/H_2O photo-conversion system with the CotpyP-loaded $SrTiO_3$:La,Rh|Au|RuO_2-$BiVO_4$:Mo photocatalysts (adapted from ref. [58] with permission from Springer Nature). (c) Sketch map of Z-scheme model and light-induced charge transfer path over SiC@MoS_2 photocatalyst (adapted from ref. [59] with permission from ACS Publications). (d) CO_2/H_2O photo-conversion reaction route of the heterometallic cluster-based organic frame photocatalyst (adapted from ref. [60] with permission from Wiley-VCH). (e) Diagrammatic sketch of water splitting on Pt nanoparticle (gray) decorated CdS (yellow) (adapted from ref. [31] with permission from Springer Nature).

photocatalysts have excellent visible light absorption and almost ideal energy band structure, non-single crystal or haploid Ta_3N_5 can barely achieve overall water splitting due to the strong charge recombination at defects. Domen's group fabricated Ta_3N_5 nanorods growing on lattice-matched cubic $KTaO_3$ particles, combined with the Rh/Cr_2O_3 cocatalyst. Since the single-crystal Ta_3N_5 nanorod crystals had few grain boundaries, the materials presented high water-splitting efficiency under simulated sunlight [33].

Molecular composites are also effective photocatalytic materials for achieving scalable and sustainable carbon dioxide reduction. Reisner's group prepared a photocatalytic sheet by integrating La and Rh co-doped $SrTiO_3$, Mo-doped $BiVO_4$, phosphonated Co(ii) bis(terpyridine) and RuO_2 catalysts onto a gold layer [58] (Fig. 3b). This device achieves a solar energy conversion (from CO_2 to formate) efficiency of 0.08 ± 0.01% and a selectivity of 97 ± 3%, respectively. When the device was exposed to simulated sunlight, e^-–h^+ pairs were produced in both $SrTiO_3$: La, Rh and $BiVO_4$: Mo. Electrons were transformed from $BiVO_4$:Mo conduction band to the $SrTiO_3$:La,Rh donor level through the Au layer. With the aid of molecular compounds, e^- in $SrTiO_3$: La,Rh reduced CO_2 into $HCOO^-$, simultaneously h^+ in the $BiVO_4$:Mo oxidized H_2O to O_2 with RuO_2 cocatalyst for O_2 generation.

The Z-scheme heterojunction can be propitious to the transfer balance of photogenerated e^-–h^+ pairs. Li's group realized the overall CO_2/H_2O conversion through marigold-like SiC@MoS_2 nanoflower materials with 323 $\mu L\,g^{-1}\,h^{-1}$ methane yield and 620 $\mu L\,g^{-1}\,h^{-1}$ O_2 release under $\lambda \geq 420$ nm visible light irradiation. This photocatalytic performance can be ascribed to the following aspects: (i) the direct Z-scheme heterostructure with negative SiC conduction band for CO_2 reduction and positive MoS_2 valence band for O_2 evolution, (ii) the high e^- mobility of SiC and high h^+ mobility of MoS_2, (iii) the marigold flower-like microstructure of SiC@MoS_2 making the surface of catalyst completely exposed to reactants and (iv) the gas–solid reaction beneficial to adsorption/desorption behavior on the Z-scheme heterostructure surface [59] (Fig. 3c).

Through reasonable material design, appropriate doping modification and deposition of cocatalysts, the feasibility of free charge recombination losses for efficient overall water splitting can be achieved. Domen's group demonstrated overall water splitting, evolving H_2 and O_2 in a 2 : 1 stoichiometric ratio at an external quantum efficiency up to 96% (350 nm $< \lambda <$ 360 nm), using Al doped $SrTiO_3$ photocatalysts [35]. By selectively photo-depositing the cocatalysts Rh/Cr_2O_3 for H_2 evolution and cobalt hydroxide oxide (CoOOH) for O_2 generation respectively, the H_2 and O_2 evolution could be enhanced separately by anisotropic charge transport on different crystallographic planes of the catalyst particles.

A system with clear structure to clarify the relationship between structure and photosynthesis is very important in promoting the development of artificial photosynthesis. Lan and Liu synthesized metal organic framework (MOF) photocatalysts based on heterometallic Fe_2M clusters. The catalysts converted carbon dioxide and water into formate and O_2 without additional sacrificial agents and photosensitizers. Visible light excited heterometallic clusters and photosensitive ligands to produce photo-generated electron-hole pairs. Low-cost metals accepted electrons to reduce carbon dioxide,

while high-price metals used holes to oxidize water [60] (Fig. 3d). Lan and Liu's work proposed a novel strategy of designing crystalline catalysts for overall artificial photosynthesis.

The combination of catalysts that are of nanometer and molecular scale is of great significance in visible-light-induced overall artificial photosynthesis. Stolarczyk's group put forward the design idea of 'all in one'. Spatial separation of oxidation and reduction sites respectively on CdS nanorods and the co-modification parts of the both sites, i.e. Pt nanoparticles and $Ru(tpy)(bpy)Cl_2$-based molecules, was realized [31] (Fig. 3e). Pt nanoparticles at the tip of CdS nanorods acted as electron receptors and were responsible for H_2 production ($20\ \mu mol\ g_{cat}^{-1}\ h^{-1}$). $Ru(tpy)(bpy)Cl_2$-based molecular cocatalysts were fixed to the periphery of CdS nanorods and are responsible for O_2 production ($170\ \mu mol\ g_{cat}^{-1}\ h^{-1}$). The catalyst has both reduction and oxidation catalytic functions, so that visible light can drive the total water splitting without sacrificial agents.

Generally speaking, in the last decade, great progress has been made on photocatalytic CO_2RR. The solar energy conversion efficiency of photocatalytic materials has gradually improved; the methods to improve the photocatalytic reaction efficiency tend to be clear; the understanding of the photocatalytic mechanism has gradually deepened; the characterization methods are developing rapidly; and photocatalytic materials based on novel physical mechanisms are emerging. However, in order to achieve the practical goals of EAP, the research on CO_2RR still needs a leap forward. First of all, one of the key problems is how to greatly improve the photocatalytic CO_2RR performance. In addition to the requirement to develop new materials, how to match the band gap of photocatalytic materials with the extraterrestrial solar spectrum, how to match the conduction/valence band position of EAP materials with the potential of reactants, how to reduce electron-hole recombination and improve quantum efficiency, and how to improve the stability of photocatalytic materials are still key scientific issues that must be solved in this field. Secondly, existing characterization techniques cannot fully facilitate an understanding of the catalytic mechanism. Thus, some advanced *in-situ* and/or atomic level characterization methods are still required to reveal the key factors affecting the photocatalytic reaction process. As for realizing efficient and stable EAP, researchers need to deepen the understanding of the photocatalytic reaction mechanism from a macroscopic and qualitative description to microscopic and quantitative research, to comprehensively study the process of light absorption, electron-hole excitation and transport, and interface dynamics, and to clarify the mechanism of energy transfer and conversion. These approaches can guide researchers when it comes to developing EAP materials with high quantum efficiency, by breaking through the existing theoretical framework and actively promoting the cross-integration of photochemistry and other disciplines.

Photoelectrocatalysis materials for EAP

Photocatalytic overall CO_2/H_2O conversion materials are mainly in the form of powders. There are problems such as the undesirable recombination of photo-generated electron-hole pairs in the particles and difficult separation of products from the system. Thus, photoelectrocatalysis, especially non-biased photoelectrocatalysis, in which the catalysts are in the form of film, is more beneficial to the practical applications of EAP.

Photoelectrochemical artificial photosynthesis is generally carried out by photoelectrodes composed of conductive substrates, semiconductors and co-catalysts in the aqueous environment. In this system, the excited photoelectrodes generate electrons or holes that migrate to the surface of the photocathodes or photoanodes for a reductive or oxidation reaction, respectively. Compared with the fact that the charge separation driving force of photocatalysts is the built-in electric field, charge separation in photoelectrocatalytic systems is promoted not only by a built-in electric field but also through external bias. Therefore, some thermodynamically insufficient catalytic reactions can be carried out under photoelectrocatalytic systems with proper bias. In addition, photoelectrocatalysis realizes the spatial separation of the reduction reaction and oxidation reaction to avoid the inverse reaction. According to the module composition of each part of the system, the photoelectrocatalysis system can be divided into a photocathode-to-electrode system, photoanode-to-electrode system, photocathode-photoanode system and photovoltaic coupled photoelectrocatalysis system.

A photocathode usually consists of p-type semiconductors. The conductive band of a p-type semiconductor bends downward at the interface of semiconductor and solution. This band bending allows photo-generated electrons to migrate to the electrode/solution interface and the electrons participate in the CO_2 reduction reaction to produce hydrocarbon fuel. According to the thermodynamic requirements, the main photocathode materials are Cu_2O [49], Cu_2ZnSnS_4 [50], Co_2P and p-Si [51].

Correspondingly, a photoanode usually consists of n-type semiconductors. The valence band of an n-type semiconductor bends upward at the semiconductor/solution interface, allowing

photo-generated holes to transfer to the electrolyte for O_2 evolution. The main photoanode materials are TiO_2, Fe_2O_3, WO_3, ZnO, $BiVO_4$, Ta_3N_5 and n-Si [3,61–66].

It is usually difficult to construct a device that has an individual photoelectrode and can achieve both CO_2 reduction and water oxidation conversion for overall artificial photosynthesis (Fig. 1d). The construction of a dual photoelectrode system with both the photocathode and photoanode is beneficial for realizing the full conversion of artificial photosynthesis without bias. The difference in Fermi level between two photoelectrodes determines the theoretical maximum of the photo-generated voltage between them [58,59], which should be larger than the thermodynamic and kinetic requirements.

The photovoltaic coupling system is also used to couple photovoltaic cells to the photoelectrocatalytic system to make effective artificial photosynthetic systems, in which the photovoltaic cell provides bias to assist in driving electrocatalytic reactions. This kind of system includes photovoltaic-photocathode, photovoltaic-photoanode and photovoltaic-electrocatalytic coupling systems (Fig. 1e).

As mentioned above, the photocathode catalysts, photoanode catalysts and photovoltaic electrodes together form the most important material basis in photo-electrocatalytic systems for EAP. Thus, the research progress of photocathode catalysts, photoanode catalysts and photovoltaic electrodes appropriate for EAP will be discussed as follows.

Photocathode materials

Numerous p-type semiconductors have been exploited and investigated for photocathodes, including p-type silicon [67], oxides [68–73], sulfides [74], phosphides [67] and selenides [75]. Tellurides [76] have been investigated for CO_2 reduction or H_2O reduction. In addition, profiting from remarkable CO_2/H_2O molecular adsorption and activation, cocatalysts (e.g. Pd, Au, Ag and Cu) [77] usually serve as photocathodes. However, their performance is still limited by high overpotential, low selectivity and long-term operational instability [78]. Rational design is needed to optimize the material interface to achieve efficient charge transfer at low overpotential while maintaining high selectivity.

P-Si is one of the most popular materials for photocathodes, not only because of its high earth reservation, but more importantly, Si has a proper valence band position, with a 1.1 eV band gap. However, its CO_2 reduction activity is low, and it lacks a suitable cocatalyst to improve the effect. For planar Si electrodes, the overpotential of CO_2 reduction on the surface is mainly reduced by loading metal cocatalysts [79,80]. Recently, the loading of non-noble metal cocatalysts such as MoS_2 [81] reduced graphene oxide (rGO) [82], NiO_x [83] and Al_2O_3 [84] has been found to further improve the stability of Si in the water decomposition process of photoelectrochemical cells (PECs). For example, Bench *et al.* deposited a MoS_2 thin layer on the surface of an Si photocathode with n^+p planar structure, and the photocathode could be stable in electrolyte for >100 h [81]. Si nanowires are also widely used in the construction of photocathodes. The main reason is that Si is a typical indirect band gap semiconductor, and its high light absorption efficiency can be ensured when the penetration depth of light reaches 200 μm. The nanowire structure can reduce the migration distance of minority carriers, and multiple reflections of light can ensure the effective absorption of light by Si [85]. Photolithography technology was used to etch and form Si nanopillar arrays on Si wafers, which increased the contact area between photocathode and electrolyte. After Mo_3S_4 nanoclusters were deposited on the surface of p-Si, the light absorption range of the material was widened to over 620 nm, and reached a highly increased current density [86]. Recently, Chen *et al.* modified MoS_2 with band gap position matching p-Si arrays as the cocatalyst, and used it to collect photo-generated electrons to reduce carrier recombination. Therefore, the initial H_2 evolution potential of an Si@MoS_2 photocathode is positively shifted to 0.122 V vs. reversible hydrogen electrode (RHE). The researchers further doped MoS_2 with metal atoms to construct an Si@$MMoS_x$ (M = Fe, Co, Ni) photocathode. It was found that the initial H_2 evolution potential of the material moved positively to 0.192 V vs. RHE after Co doping, and the current density at 0 V vs. RHE reached -17.2 mA cm^{-2} [87]. Jin *et al.* supported a transparent $NiCoSe_x$ thin layer on the surface of a bamboo-shoot-like Si nano-array by photo-assisted electrodeposition (Fig. 4a) [88]. Under 100 mW cm^{-2} sunlight intensity, the current density of the catalyst at 0 V vs. RHE reached -37.5 mA cm^{-2}. In addition, Hu Xile's research group combined Mo_2C with amorphous Si and tested it as photocathode in 1 M KOH and 0.1 M H_2SO_4. The stable photocurrent density of this material in both electrolytes can reach -11 mA cm^{-2}. This is the first time that the Si-based photocathode has been used in strong alkaline electrolyte, and is also the Si-based photocathode material with the widest pH range so far [89]. Besides, n-type doping on the surface can control the band bending of p-Si and form an n+p depletion layer, thus

increasing the photovoltage of the p-Si photocathode. However, the direct contact between n+p-Si and metal catalysts generally causes serious surface recombination and reduced photovoltage. Inserting a metal oxide layer between the Si and catalysts to form a heterojunction can effectively adjust the charge transfer from semiconductor to cocatalysts. CO_2 reduction in a silicon photocathode was reported to be realized by depositing TiO_2 through p^+ implantation and n^+ implantation on the illumination side, and then loading the Ag/dendritic Cu catalyst. A self-powered CO_2 reduction device is formed by tandemly coupling the silicon photocathode with two series of translucent $CH_3NH_3PbI_3$ perovskite solar cells, and the conversion efficiency from sunlight to hydrocarbon and oxygen-containing compounds is 1.5%. Under simulated sunlight conditions, the efficiency of photocathode to hydrocarbons and oxygenated compounds (mainly ethylene, ethanol and propanol) is kept above 60%, which can last for more than several days (Fig. 4b) [90].

Metal oxide semiconductors (such as binary oxide Cu_2O (2.0 eV)) and ternary oxides (for instance, $CaFe_2O_4$ (1.9 eV), $CuNb_3O_8$ (1.5 eV), $CuFeO_2$ (1.5 eV) and $LaFeO_3$) are typical p-type semiconductors due to metal vacancies in the structure. Metal oxide semiconductors are extensively utilized for the design and synthesis of photocathode materials because of their easy preparation and low cost. However, their unsatisfactory optical absorption coefficient, carrier mobility and stability make the energy conversion efficiency of oxide photocathodes relatively low [68–73]. Cu_2O is a typical representative of this type of material and considered as a promising photocathode material to replace Si [91–93]. However, poor stability is the main problem for Cu_2O-based photocathodes (Fig. 4c) [94]. Grätzel's group has done a series of work to improve the stability of Cu_2O-based photocathodes. They used MoS_{2+x} film as a hydrogen evolution reaction (HER) catalyst on the TiO_2-protected Cu_2O photocathode, and the current density of the composite electrode could reach -5.7 mA cm^{-2} (0 V vs. RHE) [95]. After that, they deposited a double layer Al :ZnO/TiO_2 film on the Cu_2O surface and its improved activity was mainly attributed to the matched conduction band position of Cu_2O, ZnO and TiO_2, leading to quick electron migration from electrode to electrolyte [96]. As the best-performing oxide photocathode, the Cu_2O photocathode's activity surpasses that of many photocathodes after continuous research and development. However, Cu_2O photocathodes employing Au as the back contact generally caused considerable e^-–h^+ recombination. By employing CuSCN as the h^+ transport material, h^+ transport between Cu_2O and CuSCN is expedited by band-tail states, delivering a 4.55% solar-to-hydrogen (STH) efficiency (Fig. 4d) [97].

p-NiO is also a type of electrode material for CO_2 reduction PECs. DuChene *et al.* investigated the light-induced modulation of catalytic selectivity over Cu/p-type NiO photocathodes. According to their analysis, the optical excited hot e^- of Cu nanoparticles were mainly used for CO_2 reduction, while hot h^+ injection from Cu nanoparticles into p-type NiO leads to charge separation. Thus, the optical excitation of plasmonic Cu/p-type NiO photocathodes enhanced CO_2 reduction and inhibited H_2 evolution, driving increased production of CO and HCOOH. This work demonstrated a plasmon-driven photocathode for CO_2 reduction PECs (Fig. 4e) [98].

$CuIn_xGa_{1-x}Se_2$ (CIGS, 1.0–1.68 eV) and Cu_2ZnSnS_4 (CZTS, 1.0–1.5 eV) perform outstandingly in the field of solar cells due to their high light absorption coefficient ($\sim$105 cm^{-1}) and adjustable direct band gap. The modulation of chemical composition (I = Cu, Ag; II = Al, In, Ga; VI = S, Se, Te) makes the band gap of such a semiconductor adjustable within 1.0–2.4 eV. Furthermore, because of the inherent metal defects (such as Cu vacancy), this type of semiconductors are typical p-type semiconductors, which can be used as a photocathode material. CIGS photocathodes with high current density, such as $CuGaSe_2$ (1.7 eV), $CuGa_3Se_5$ (1.8 eV) and $CuInS_2$ (1.5 eV), have also been reported in recent years. However, the lattice mismatch at the interface limits the energy conversion efficiency of this kind of material. CdS film prepared by chemical bath deposition (CBD) is one of the best n-type semiconductors reported to compound CIGS to form a p–n junction. However, these materials were difficult in terms of application because of their slow surface reaction process and poor stability in aqueous solution [99]. Therefore, depositing a protective layer on the surface is the most important means to solve the above problems. Sb_2Se_3 can also be a promising material for artificial photosynthesis. Yang *et al.* reported an Sb_2Se_3 photocathode material with low cost, small band gap and good photoelectric properties and photocorrosion stability, which also showed a high current density of almost 30 mA cm^{-2} at 0 V vs. RHE. The optimized Sb_2Se_3 photocathode achieved 1.5% solar-to-hydrogen efficiency for unassisted water splitting under the condition of 1 sun simulation when combined with a $BiVO_4$ photoanode, and the stability exceeded 10 hours (Fig. 4f) [100].

Some traditional cocatalysts (like Ag) are great electrocatalysts for CO_2-to-CO conversion. However, high overpotential limits the efficiency and

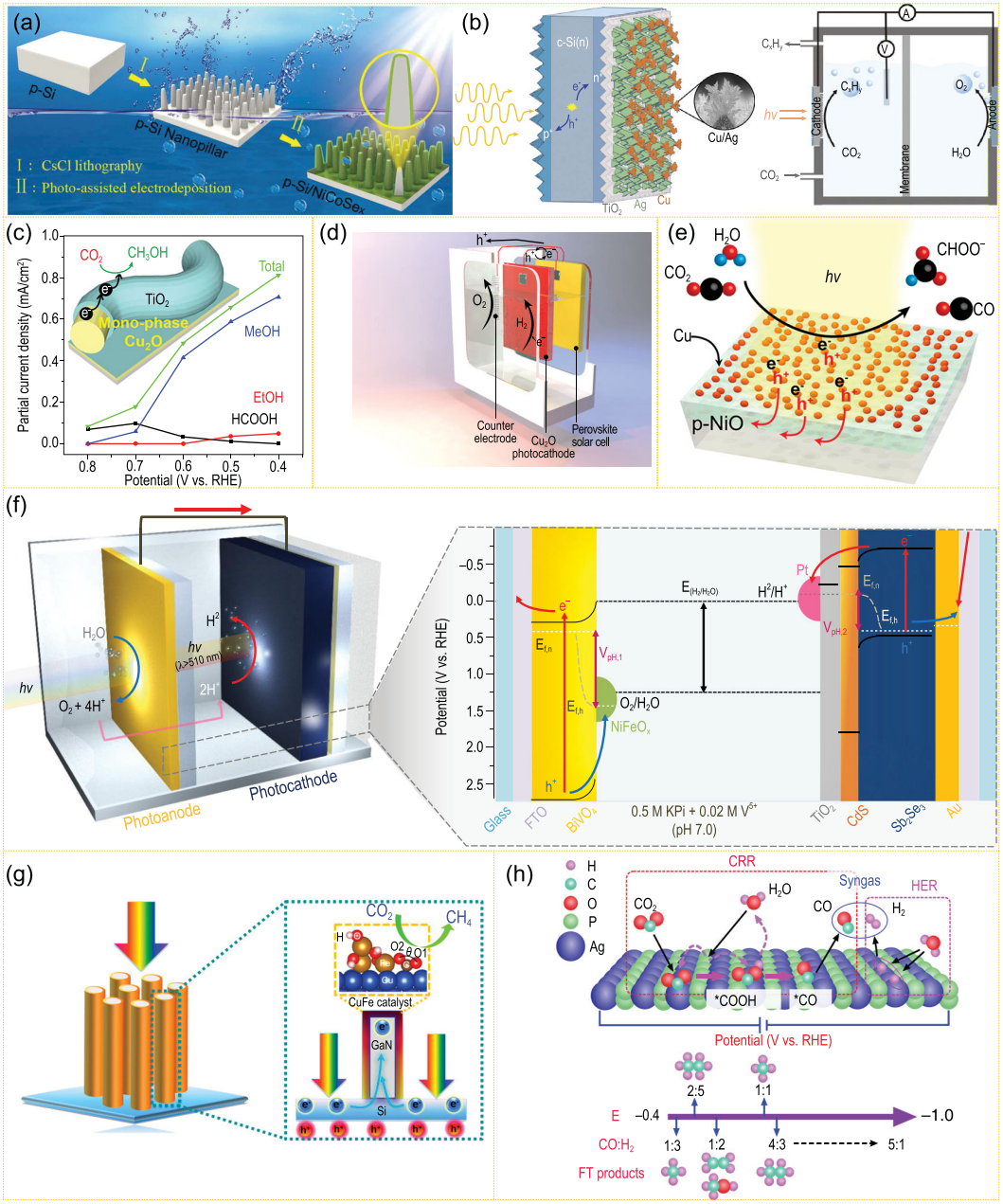

Figure 4. (a) Schematic diagram of the construction process of the p-Si/$NiCoSe_x$ photocathode (adapted from ref. [88] with permission from the Royal Society of Chemistry). (b) Left: schematic of the Si/TiO_2/Ag/Cu photocathode. Right: schematic of the membrane-separated photoelectrochemical cell (PEC) for overall CO_2/H_2O conversion (adapted from ref. [90] with permission from the Royal Society of Chemistry). (c) Diagrammatic sketch of the Cu_2O nanofiber electrode with a Cu_2O underlayer and a TiO_2 passivation layer and its CO_2 photo-reduction performance (adapted from ref. [94] with permission from ACS Publications). (d) A photovoltaic (PV)-PEC system based on CuSCN/Cu_2O photocathode and perovskite solar cell/IrO_x anode for overall H_2O splitting (adapted from ref. [97] with permission from Springer Nature). (e) Plasmonic Cu/p-NiO photocathodes for CO_2/H_2O conversion (adapted from ref. [98] with permission from ACS Publications). (f) Scheme of the $NiFeO_x$/Mo:$BiVO_4$/FTO||Pt/TiO_2/CdS/Sb_2Se_3/Au/FTO cell for total water splitting (adapted from ref. [100] with permission from Springer Nature). (g) Spatial decoupling of CO_2 reduction from light absorption and charge separation over CuFe@GaN NWs/Si (adapted from ref. [101] with permission from the National Academy of Sciences, USA). (h) Schematic diagram of selective CO_2-to-syngas on AgP_2 (211) (adapted from ref. [102] with permission from Springer Nature).

the lack of efficient and highly selective cocatalysts restricts the PEC performance of photocathode catalysts. To solve the problem of unsatisfied efficiency resulted from high overpotential, a few ingenious cocatalysts have been designed and present a promising avenue for photocathode catalysts, such as CuFe alloy and AgP_2. The designed CuFe was reported to exhibit a -38.3 mA cm^{-2} current density with CH_4 faradaic efficiency up to 51%, resulting in a 2176 h^{-1} turnover frequency using silicon as photocathode under one sun illumination (AM 1.5G) (Fig. 4g) [101]. Integrating AgP_2 nanocrystal cocatalysts on n^+p-Si to construct an n^+p-Si/Al_2O_3/AgP_2 hybrid photocathode and separating the n^+p-Si and AgP_2 by the Al_2O_3 layer led to a highly improved CO_2 conversion efficiency. Compared with the Ag cocatalyst, the overpotential of AgP_2 nanocrystals for CO_2 reduction to CO is reduced by 0.3 V, and the maximum faradaic efficiency is 82% (Fig. 4h) [102].

Photoanode materials

Generally, the anodic reaction is an OER in a PEC, which is a vital reaction in extraterrestrial space for human respiration. The photoanode OER is a four-electron transfer process with slow reaction kinetics, which is the rate control step of the artificial synthesis process. Therefore, photoanode materials with high activity and stability are indispensable in improving the energy conversion efficiency of PEC systems for EAP. Numerous n-type semiconductors have been exploited and investigated, including n-type silicon [66], oxides [61–64], nitrides [103] and sulfides [104], as photoanodes for O_2 production. In addition, finely dispersed cocatalyst nanoparticles (e.g. Co [61], Fe [66]), phosphides [105] and hydroxyapatite [106], or conformal thin layers of cocatalysts (e.g. oxyhydroxide, sulfides) [107] on the photoanode surface are also an effective approach for remarkable O_2 generation. Among the diverse catalysts, TiO_2, WO_3, Fe_2O_3 and $BiVO_4$ with befitting band structure and plummy stability of aqueous solution, are good n-type semiconductor photoanode materials for O_2 production through water oxidation [3,61–63]. At present, the O_2 production of unmodified individual photoanode materials still needs to be improved, mainly due to poor surface reaction kinetics and weak carrier separation and transport. Many studies have improved the above problems by surface modification or defect regulation, design of heterojunction, rational design of cocatalyst, and so forth.

Recent research progress on the study of TiO_2 and $BiVO_4$ photoanodes is introduced below. Surface modification and heterojunction construction have been used for improving TiO_2 photoanode performance. The Ti-OH surface states produced by electrochemical doping on the photoanode of TiO_2 nanotubes, leading to charge-separation-efficiency increase, contributes to the water oxidation [108]. Heterojunction construction of the g-C_3N_4 film on the TiO_2 nanorod array exhibits obvious advantages in PEC performance (Fig. 5a) [103].

The design of heterojunction and oxygen vacancy defects is demonstrated to be a synergetic method of producing a high performance in photoanodes. Integration of Fe_xS and the synchronous generation of interfacial oxygen vacancies (V_O) synergistically reduced the carrier recombination, increased the number of active sites and facilitated the participation of photo-generated holes in water oxidation for the Fe_2O_3 photoanode (Fig. 5b) [104]. Lianzhou Wang *et al.* reported a synergetic $BiVO_4$ film rich in *in-situ*-formed oxygen vacancy defects converted from Bi_2S_3 precursor films through a sulfur oxidation method, in which the electron-hole separation rate of the bulk phase was significantly improved. $NiFeO_x$ O_2-evolution cocatalysts were supported on the photocatalyst surface to facilitate surface O_2 evolution. A 5.54 mA cm^{-2} photocurrent density was obtained under 1.23 V vs. RHE and simulated sunlight (AM 1.5), with a stability over 80 h. A 6.24 mA cm^{-2} photocurrent density can be obtained by stacking two $BiVO_4$/$NiFeO_x$ electrodes, and the photoelectric conversion efficiency reaches 2.76% [109]. Bi *et al.* also enhanced the O_2 production activity of the $BiVO_4$ photoanode under a similar mechanism by depositing a 2 nm β-FeOOH film with abundant oxygen vacancies (Fig. 5c) [110].

In addition, for most of the photoanode materials, ingenuity in cocatalyst design has been proven to ameliorate the OER. The selective growth of FeNi cocatalysts on the $BiVO_4$ photoanode surface obviously raised the photocurrent density to 5.8 mA cm^{-2} under 1.23 V vs. RHE and simulated sunlight (AM 1.5) (Fig. 5d) [111]. The selective formation of interfacial bonds between Fe, Ni in FeNi cocatalysts and Bi, V on the surface of the $BiVO_4$, implied that after optical excitation, Fe-O-Bi interface bonding can effectively transfer the photo-induced holes from $BiVO_4$ to Fe active sites. The photo-induced electronic injection will be delivered from Ni atoms to V sites through the Ni-O-V, thus effectively avoiding the V^{5+} ion dissolution. The introduction of Fe species can significantly improve its water-oxidation activity, while Ni can effectively enhance its photoelectric catalytic stability. Inserting black phosphorene (BP) between the OER cocatalyst (NiOOH, MnO_x or CoOOH) and $BiVO_4$ was reported to improve the PEC performance by 1.2–1.6-fold [112], and a 4.48 mA cm^{-2} photocurrent density at 1.23 V vs. RHE was achieved by

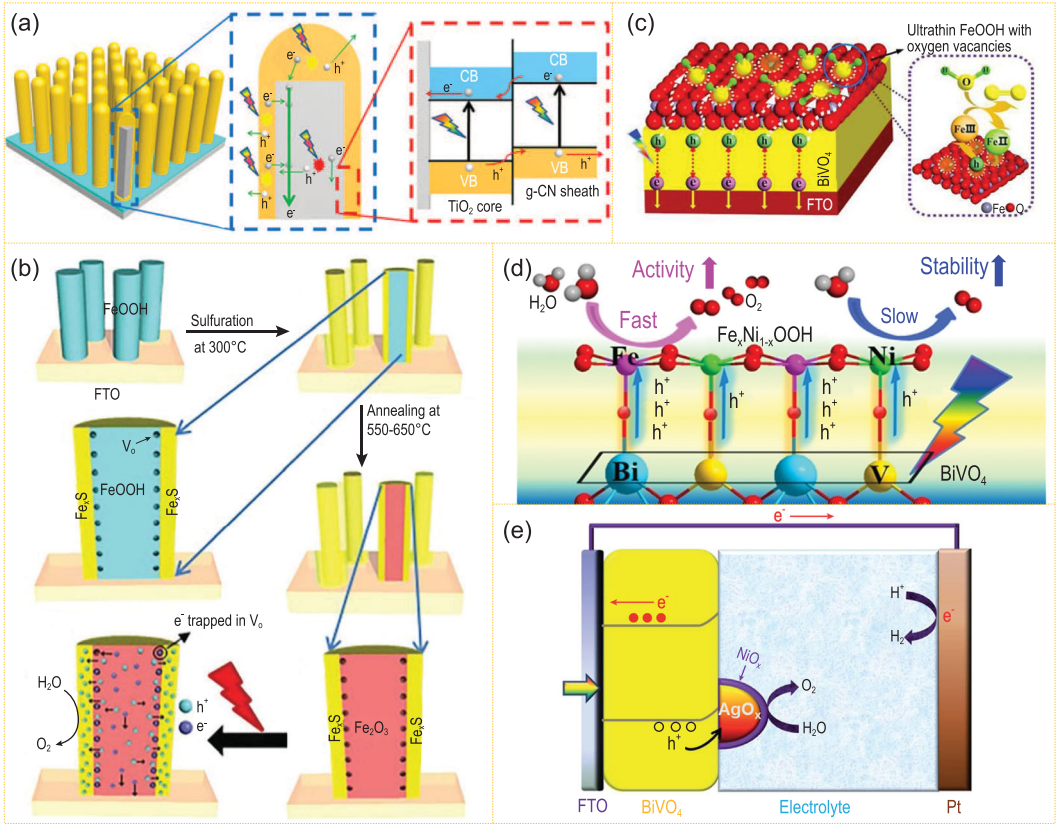

Figure 5. (a) Schematic of the energy diagrams and PEC system of the TiO_2@*g*-C_3N_4 (adapted from ref. [103] with permission from the Royal Society of Chemistry). (b) Diagram of the construction of Fe_2O_3/interfacial V_O/Fe_xS photoanode and its catalytic mechanism (adapted from ref. [104] with permission from the Royal Society of Chemistry). (c) Illustration of charge transfer during the catalytic process on β-FeOOH/$BiVO_4$ photoanode (adapted from ref. [110] with permission from Wiley-VCH). (d) Catalytic mechanism on $BiVO_4$/$Fe_xNi_{1-x}OOH$ photoanode (adapted from ref. [111] with permission from Wiley-VCH). (e) Mechanism of solar H_2O splitting over $BiVO_4$/AgO_x/NiO_x photoanode (adapted from ref. [113] with permission from the Royal Society of Chemistry).

the NiOOH/BP/$BiVO_4$ photoanode. The intrinsic p-type BP can enhance h^+ extraction and the h^+ trapping lifetime on the $BiVO_4$ surface, while the OER cocatalyst overlayer can suppress catalyst self-oxidation for achieving a high durability. This research presents an advantageous nexus between cocatalyst and semiconductor. AgO_x/NiO_x composite cocatalysts can be exploited to hoist the H_2O oxidation kinetics, as well as the carrier separation of $BiVO_4$ photoanodes, because of the high-valence-state stabilization of the metal ions, the formation of H_2O oxidation active sites and the extension of the band bending region induced by AgO_x/NiO_x (Fig. 5e) [113].

Photovoltaic (photo)electrocatalytic materials

Compared with powder photocatalysis, photoelectrocatalysis constructs the macro-space separation of oxidation and reduction half reactions, which is beneficial to the separation of catalytic products. However, for higher catalytic performance, photoelectrocatalysis depends on the input of external electric energy. Recently, photovoltaic cells have been applied for photoelectric conversion, and the photovoltaic-electrocatalytic CO_2/H_2O conversion technology has also been greatly developed. Photovoltaic (photo)electrocatalytic overall CO_2/H_2O conversion with high efficiency provides an effective avenue for storing solar energy, which can greatly benefit EAP.

Solar cells are mainly categorized into silicon-based, III–V-based or perovskite-based photovoltaic electrocatalytic devices [114]. As high operational current densities are demanded in photovoltaic electrocatalytic devices, high-quality electrocatalysts (e.g. Au, Pt, IrO_x) are preferred. Commercial noble-metal-based electrodes such as IrO_2 (for O_2 evolution) and Au (for CO_2 reduction) [115] were successfully used for overcoming the sluggish kinetics of CO_2 reduction and O_2 evolution, respectively, which hinder the extensive implementation of overall CO_2/H_2O conversion. However, the moderate performance limits the total

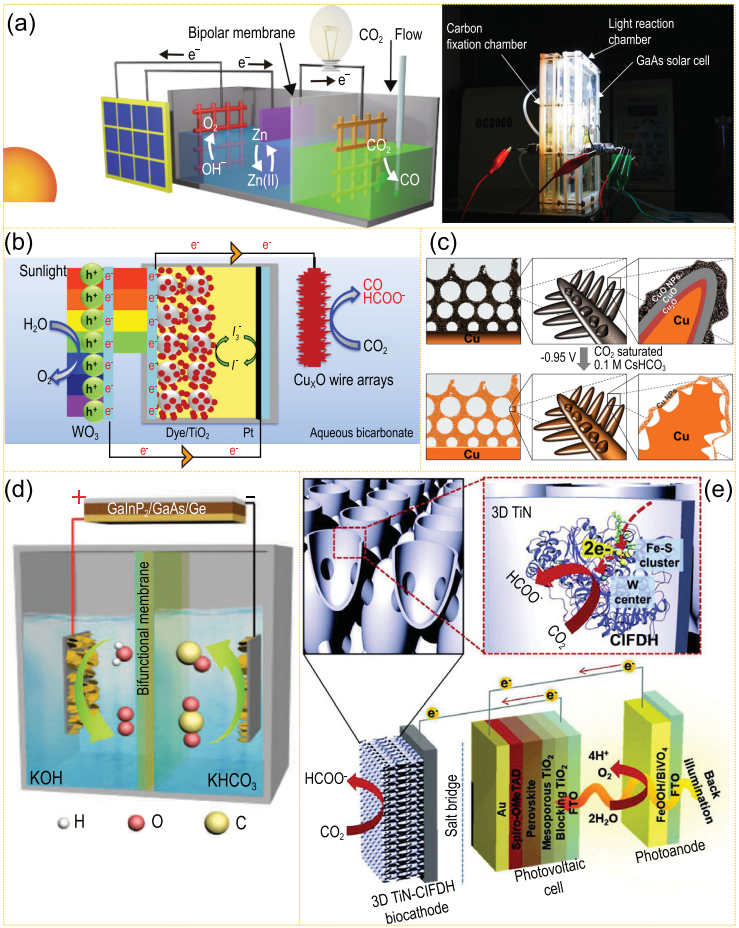

Figure 6. (a) Schematic and photograph of the redox-medium-assisted CO_2 photovoltaic electrocatalytic reduction system containing a nickel-iron hydroxide electrode and a zinc/zincate redox with a gold nanocatalyst (adapted from ref. [116] with permission from Springer Nature). (b) Illustration of a WO_3 (photoanode)||Cu_xO (photocathode) system coupling with a dye-sensitized solar cell (adapted from ref. [117] with permission from Elsevier). (c) Schematic view of the dendritic nanostructured CuO material before (top) and after (bottom) CO_2 photovoltaic electrocatalytic reduction in 0.1 M $CsHCO_3$ (adapted from ref. [118] with permission from the National Academy of Sciences, USA). (d) Illustration of the solar-driven overall CO_2 splitting system with Co_2FeO_4 nanoarrays both as anode and cathode (adapted from ref. [119] with permission from Wiley-VCH). (e) Schematic illustration of the $BiVO_4$/perovskite/3D TiN-ClFDH biocatalytic tandem PEC system for unbiased, solar-driven formate production (adapted from ref. [120] with permission from Wiley-VCH).

efficiency, and resource scarcity increases the cost. Therefore, taking further consideration of economy, resource abundance and high product selectivity, more cost-effective materials, such as Fe, Ni, Zn, W, Cu, Co or Ti-based materials, are research hotspots. The products of artificial photosynthesis are developed gradually to obtain non-toxic fuels rather than CO.

Recently, Zheng *et al.* constructed a GaAs solar cell with a nickel-iron hydroxide electrode for H_2O oxidation, and Au nanocatalysts to reduce CO_2 to CO, between which a Zn/Zn^{2+} redox medium was used for optimized charge transfer. This redox medium auxiliary system can achieve 15.6% solar energy-carbon monoxide photoelectric conversion efficiency and 63% electric energy efficiency under one sun intensity (Fig. 6a) [116]. Park *et al.* constructed a WO_3 photoanode and Cu_xO photocathode system coupled with a dye-sensitized solar cell for driving CO_2 reduction on Cu_xO and water oxidation on WO_3 with zero external bias. In this dual-light-absorbing cell, the solar-to-chemical energy efficiency of CO_2 reduction for CO is 2.5%, while it is 0.7% for H_2 and 0.25% for HCOOH, respectively (Fig. 6b) [117]. By using Cu-based catalysts at both anode and cathode coupled with a perovskite photovoltaic mini-module, Fontecave *et al.* reported a 21% energy efficiency and a 2.3% solar-to-hydrocarbon efficiency of CO_2 reduction to $CH_2{=}CH_2$ and CH_3CH_3 (Fig. 6c) [118]. By using Co_2FeO_4 nanosheet arrays for both cathode and anode, driven by a $GaInP_2/GaAs/Ge$ photovoltaic cell, Cao *et al.* showed a complete overall CO_2/H_2O conversion system with 13.1 mA cm^{-2} photocurrent density, corresponding to 15.5% solar-to-CO efficiency (Fig. 6d) [119]. The dual functional attributes can be attributed to the formation of *COOH and *O intermediates that originated from the Co sites in Co_2FeO_4. Lee *et al.* reported an enzyme—W-containing formate dehydrogenase (FDH) from *Clostridium ljungdahlii* (ClFDH)-conjugated direct electron transfer-type biocathode based on TiN nanoshell—and applied it to a PV-PEC system with free bias, which showed promising and stable solar-driven CO_2-to-HCOOH conversion at a rate of 0.78 μmol h^{-1} for 24 h and a 77.3% faraday efficiency (Fig. 6e) [120].

Although the research history of the photoelectrocatalytic CO_2 reduction reaction has been developed over tens of years with great progress, there are still many problems and challenges. Because of the low catalytic efficiency, it is far from meeting the requirements of EAP application:

(i) The selectivity of high carbon products is still very low. In CO_2RR, although the faraday efficiency of CO and HCOOH can reach >90%, the highest faraday efficiencies of other reduction products, which are much more desired for EAP technology, such as CH_4, CH_3OH, C_2H_5OH, CH_3COOH and C_2H_4, are only at the level of ∼50%.

(ii) The catalysts have poor stability. Stability is an important parameter to characterize the advantages and disadvantages of a catalyst material, and it is also a problem that must be overcome to realize EAP in harsh extraterrestrial environments. Although some catalytic materials remain stable for hundreds of hours, they are still far from the

Table 1. More specific and detailed information about the example references.

Method	Catalyst	Reactant	Light source/intensity	Current densities	Product/selectivity	TOF	Efficiency	Ref.
Photocatalysis	$4.5(ZnGa_2O_4):(Zn_2GeO_4)$	CO_2, 0.4 mL deionized water	A UV-enhanced (200 to 350 nm) 300 W xenon arc lamp	-	0.5 μmol h^{-1} CH_4, 3 μmol h^{-1} O_2	-	-	[52]
	CeO_2 octahedron textured with nanorods	CO_2, 0.4 mL deionized water	300 W Xe lamp (full spectrum)	-	0.86 μmol h^{-1} g^{-1} CH_4, ~2 : 1 molar ratio of O_2 to CH_4	-	CH_4 quantum efficiency (%) = 0.2% at 380 nm	[54]
	Rh-CoO_x/GaN nanorod arrays	Pure aqueous solution	300 W Xe lamp (full spectrum)	-	H_2 and O_2 in stoichiometric ratio (2 : 1)	-	OER quantum efficiency (incident light wavelength range of 250–400 nm) reaches 81.1%, quantum efficiency of overall water splitting reaches 6.9%	[56]
	Microwave-synthesized carbon-dots decorated carbon-nitride	CO_2, 10 mL water	300 W Xe lamp ($\lambda > 420$ nm)	-	Methanol 13.9 μmol h^{-1} g^{-1}, CO 0.05 μmol h^{-1} g^{-1}, O_2 to methanol is ~1.45 : 1; 99.6% selectivity from CO_2 to methanol	-	Internal quantum efficiency (IQY) of 2.1% in the visible region	[57]
	CotpyP-loaded $SrTiO_3$:La,Rh|Au|RuO_2-$BiVO_4$:Mo photocatalyst sheet	CO_2-saturated 0.1 M $KHCO_3$	AM 1.5 G (1 sun) illumination (100 mW cm^{-2})	-	O_2 1.3 μmol h^{-1} cm^{-2}, $HCOO^-$ 16.1 μmol in 5 h	TON for $HCOO^-$ was 305 after 4 h	A solar-to-formate conversion efficiency of 0.08 ± 0.01% with a selectivity for formate of 97 ± 3%	[58]
	$SrTiO_3$:Al photo-deposited with Rh/Cr_2O_3/CoOOH		Xe lamp (300 W, full arc)	-	Overall water splitting, evolving H_2 and O_2 in a 2 : 1 stoichiometric ratio	-	An IQE of 100% and an external quantum efficiency (EQE) >50%	[35]

Table 1. *Continued.*

Method	Catalyst	Reactant	Light source/intensity	Current densities	Product/selectivity	TOF	Efficiency	Ref.
Photoelectrochemical cells	Si@$CoMoS_x$ photocathode	0.5 M H_2SO_4	500 W xenon lamp equipped with an AM 1.5 filter (100 mW cm^{-2})	−17.2 mA cm^{-2} at 0 V_{RHE}	H_2 3.86 μmol min^{-1}	-	Faradaic efficiency 81.0%	[87]
	p-Si/$NiCoS_x$ core/shell NP arrays	0.5 M H_2SO_4	AM 1.5G illumination (100 mW cm^{-2})	-37.5 mA cm^{-2} at 0 V_{RHE}	H_2	-	-	[88]
	a-Si/Mo_2C	0.1 M H_2SO_4 and 1.0 M KOH	AM 1.5G illumination (100 mW cm^{-2})	-11.2 mA cm^{-2} at 0 V_{RHE}	H_2	-	-	[89]
	An Si photocathode with two series-connected $CH_3NH_3PbI_3$ perovskite solar cells	0.1–0.5 M $CsHCO_3$	AM 1.5G illumination (100 mW cm^{-2})	No bias	Ethylene, ethanol and 1-propanol	-	Total solar-to-chemical conversion efficiency of 3.5% to all products and 1.5% to hydrocarbons and oxygenates	[90]
	MoS_{2+x} film as the HER catalyst on TiO_2-protected Cu_2O photocathode	1 M Na_2SO_4 buffered with 0.1 M K_3PO_4 (pH = 5.0)	AM 1.5G illumination (100 mW cm^{-2})	−5.7 mA cm^{-2} at 0 V_{RHE} (pH 1.0)	-	-	7% STH efficiency in a tandem cell configuration	[91]
	Cu_2O photocathode using solution-processed CuSCN as hole transport material	0.5 M Na_2SO_4 (pH = 5.0)	AM 1.5 G illumination (100 mW cm^{-2})	6.4 mA cm^{-2} at 0 V_{RHE}	-	-	STH efficiency of 4.55%	[97]
	Sb_2Se_3 photocathode with a $BiVO_4$ photoanode	0.5 M KPi buffer + 0.01 M V_2O_5 (pH = 7.0)	AM 1.5 G illumination (100 mW cm^{-2})	-	-	-	STH efficiency of 1.5% with stability over 10 h	[100]
	CuFe catalyst coupled with GaN nanowires on n^+-p silicon wafer	CO_2-purged 0.5 M $KHCO_3$ aqueous solution (pH ≈ 8.0)	AM 1.5 G illumination (100 mW cm^{-2})	−38.3 mA cm^{-2} at −1.2 V_{RHE}	CH_4 88.8 μmol h^{-1} cm^{-2}	2176 h^{-1}	Faradaic efficiency of 51%	[101]
	A photocathode consisting of a n^+p-Si wafer coated with ultrathin Al_2O_3 and AgP_2 nanocrystals	CO_2-saturated 0.5 M $KHCO_3$ solution	AM 1.5 G illumination (100 mW/cm^2)	−3.2 mA cm^{-2} at −0.11 V_{RHE}	-	-	FE_{CO} of 67% at −0.2 V vs. RHE	[102]

Table 1. *Continued.*

Method	Catalyst	Reactant	Light source/intensity	Current densities	Product/selectivity	TOF	Efficiency	Ref.
	$BiVO_4/NiFeO_x$	1 M borate buffer electrolyte containing 0.2 M Na_2SO_3	AM 1.5 G (100 mW cm^{-2})	5.54 mA cm^{-2} at 1.23 V_{RHE}	-	-	Photon-to-current efficiency of 2.76%	[109]
	Ultrathin FeOOH nanolayers with abundant oxygen vacancies on $BiVO_4$ photoanode	0.2 M Na_2SO_4 (pH = 7.0)	AM 1.5 G illumination (100 mW cm^{-2})	4.3 mA cm^{-2} at 1.23 V_{RHE}	H_2 92.3 μmol after 120 min	-	-	[110]
	$BiVO_4/Fe_xNi_{1-x}OOH$ photoanode	0.5 M K_3BO_3 electrolyte (pH = 9.5)	AM 1.5 G (100 mW cm^{-2})	5.8 mA cm^{-2} at 1.23 V_{RHE}	H_2 388 μmol, O_2 172 μmol after 3 h	-	The average incident photon to current efficiency (IPCE) of 90% at 420 nm	[111]
	NiOOH/BP/$BiVO_4$ photoanode	0.5 M phosphate buffer (KPi, pH = 7.1)	AM 1.5 G (100 mW cm^{-2})	4.48 mA cm^{-2} at 1.23 V_{RHE}	-	-	-	[112]
	$BiVO_4/AgO_x/NiO_x$ photoanode	0.2 M KBi aqueous solution (pH = 9.25)	AM 1.5 G illumination (100 mW cm^{-2})	1.24 mA cm^{-2} at 0.6 V_{RHE}		-	The average IPCE values in the 380–450 nm range increased from 22.4% to 49.3%.	[113]
Photovoltaic cell + electro-catalysis	A photovoltaic and electrocatalytic system consisting of GaAs solar cell, nano-Au catalyst cathode and NiFe hydroxide anode and Zn/Zn(II) redox medium	0.5 M CO_2-saturated $KHCO_3$ (pH = 7.2)	AM 1.5 G illumination (100 mW cm^{-2})	10 mA cm^{-2} at 1.96 V_{RHE}	-	-	FE_{co} of ~92%, a solar-to-CO photo-conversion efficiency of 15.6%, and an electric energy efficiency of 63%	[116]
	A PEC composed of WO_3/dye-sensitized solar cell and Cu_xO ($x = 1$ and 2) wire arrays as a dual-absorber photoanode and cathode	CO_2-purged 0.1 M bicarbonate aqueous solution	AM 1.5 G illumination (100 mW cm^{-2})	-	CO, H_2 and formate	-	The primary CO_2 conversion product is CO, with a solar-to-chemical energy efficiency of ~2.5%; H_2 and formate are obtained with energy efficiencies of 0.7% and 0.25%, respectively in 5 h (overall efficiency ~3.45%)	[117]

Table 1. *Continued.*

Method	Catalyst	Reactant	Light source/intensity	Current densities	Product/selectivity	TOF	Efficiency	Ref.
	A system coupling a photovoltaic cell to an electrochemical cell using the dendritic nanostructured copper oxide material at both the anode and cathode	Cathodic electrolyte: 0.1 M CO_2-saturated $CsHCO_3$ (pH = 6.8); anodic electrolyte: 0.2 M Cs_2CO_3 (pH = 11)	Without external bias and AM 1.5 G (1 sun) illumination (100 mW cm^{-2})	A stable current of 6.0 ± 0.2 mA and a potential of 2.8 ± 0.02 V	C_2H_4, C_2H_6, CO, HCOOH, H_2	-	C_2H_4 and C_2H_6 as the main products with an average faradaic yield (FY) of 40.5% (34% for C_2H_4 and 6.5% for C_2H_6), together with CO and HCOOH in 4.8% and 6.4% FY, respectively Concomitant H_2 production was 42.2% FY	[118]
	GaInP/GaAs/Ge/Co_2FeO_4 driven by a triple junction $GaInP_2$/GaAs/Ge photovoltaic cell	0.1 M CO_2-saturated $KHCO_3$	AM 1.5 G illumination (100 mW cm^{-2})	13.1 mA cm^{-2} at −1.2 V_{RHE}	-	CO	Solar-to-CO efficiency of 15.5%	[119]
	W-containing formate dehydrogenase from *Clostridium ljungdahlii* (ClFDH) on the 3D TiN nanoshell	CO_2 saturated phosphate buffer	Xe lamp (photon energy flux of 100 mW cm^{-2}, 420 nm cut-off filter)	Bias-free	Formate 0.78 μmol h^{-1}	-	Faradaic efficiency 77.3%	[120]

EAP goals. In the field of photoelectrocatalysis especially, due to the complex structure of photocatalysts/cocatalysts, high-energy radiation corrosion and other factors, the stability of photoelectrocatalytic CO_2RR is a great challenge to overcome.

(iii) The reaction process of (photo) electrocatalytic CO_2RR requires a deeper understanding. Light absorption, charge separation and interfacial reaction in the process of (photo)electrocatalytic CO_2RR not only have differences on the time scale, but are also often localized at the atomic or molecular level on the spatial scale. Therefore, for observing the (photo)electrocatalytic CO_2RR process in order to provide a reference for future theoretical analysis, transient, microregion and *in-situ* analysis methods should be utilized and developed.

With regard to the selection of the most suitable EAP technology, photocatalysis, photoelectrocatalysis and photovoltaic electrocatalysis have their individual advantages and disadvantages. EAP based on photocatalysis without an external complex device system is portable and easy to work, and therefore more adaptable to the complex extraterrestrial environment. However, its low reaction efficiency leads to low concentration of the products, with difficulties in separation and enrichment for CO_2RR and OER products. Photoelectrocatalysis with two-electrode systems has the obvious advantage of efficient product separation. However, the very low stability of semiconductor photoelectrocatalysts under high-energy radiation makes the photoelectrocatalytic process difficult to adopt currently. In comparison, the photovoltaic coupled with electrocatalysis process can realize energy storage by separating photoelectric conversion and energy-to-chemical conversion, thus being more suitable for application in the extraterrestrial environment in recent times. With the further development of semiconductor/cocatalyst materials, we believe that composite technology with two or more systems will be the trend of EAP applications. More specific and detailed information for each system can be seen in Table 1.

CONCLUSION AND PERSPECTIVE

In summary, the development of EAP materials is highly prospected. Looking at the future of space science and technology, how to achieve extraterrestrial survival and affordable and sustainable deep space exploration through EAP technology under extreme conditions, has become the common pursuit of humanity. On this frontier, there are still a series of concomitant scientific problems, such as low concentrations of CO_2/H_2O, different solar radiation intensities, ultrahigh gravity or microgravity, extreme temperatures, intense cosmic radiation, extreme pressure and ultimate vacuums. The problems that urgently need to be resolved are listed below:

(i) CO_2/H_2O photo-conversion materials with normal working ability at low atmospheric density are the linchpin for EAP. At present, research into CO_2/H_2O photo-conversion mainly focuses on atmospheric conditions with a high concentration of, or pure, CO_2. However, the concentration of CO_2 or H_2O in the extraterrestrial environment or the enclosed space inside the capsule is usually at an ultralow level or unstable state. Therefore, how to realize the enrichment and further utilization of CO_2 is one of the critical problems. Development of artificial photosynthetical materials in low CO_2 concentration environments or CO_2 collection technology may be considered as the solutions.

(ii) It is necessary to develop a photocatalytic material system suitable for withstanding different solar radiation intensities, strong cosmic radiation and Frenkel defects under extraterrestrial conditions. Due to the difference in solar radiation intensity and spectral distribution between outer space and the Earth's surface, photocatalytic materials developed for the solar spectral conditions on Earth may not work effectively and stably in the outer space environment. Therefore, it is necessary to develop new artificial photosynthetic materials suitable for cosmic radiation with a long working life, high stability, wide spectrum and responsiveness to AM0 spectra, to meet the requirements of long-term space exploration tasks. Ceramics or composites can be selected to achieve thermostability and thermal shock resistance. Metal oxides such as PbO, BaO and Bi_2O_3 with a high atomic number, or rare metallic elements, can be added to the material for radiation resistance [121].

(iii) Research into the effects of extreme temperature, ultra-vacuum and microgravity on the photochemical reaction, as well as multi-photon processes in the photochemical reaction, will give clues as to how to plan the EAP process. The increase of interfacial resistance (ohmic drop) caused by bubbles produced in the photocatalytic process will severely affect the surface coverage of electrodes. The mass transfer

process under microgravity will become more difficult, greatly reducing the energy efficiency of the system. Supersaturated gas layers formed by gas reactants and products gathered near the three-phase interfaces of electrodes have a very important negative influence on the reaction process, material transport and reaction efficiency. Therefore, it is necessary to deeply explore the diffusion and transfer process of reaction media in electrolyte under microgravity, as well as the key mechanisms of bubble nucleation, growth, interface separation, gas-liquid two-phase flow and gas-liquid separation and their influence on photocatalytic processes. In addition, the state-of-the-art technologies of ECLSS architecture as a subsystem typical of a crewed space vehicle, which provides all the necessary conditions, can be used for the control of steady temperature and pressure inside the space capsule to support the artificial photosynthetic material, devices or systems.

(iv) The photo/thermo/electric coupling catalysis mechanism needs to be deeply understood and realized by utilizing the full spectrum of solar energy, 99.9% of which is in the infrared region (43%), visible region (50%) and ultraviolet region (7%). The band gap of existing photocatalytic materials is extensively large, and most of them absorb the ultraviolet or near-ultraviolet spectrum. As a result, the utilization rate of solar energy is not high and the overall efficiency of photocatalysis is relatively low. It is necessary to explore the mechanism of solar photo/thermo/electric coupling catalysis, develop a composite photocatalytic system with multi-spectral absorption and full-spectral utilization, and improve the reaction rate of photosynthesis and photochemical conversion efficiency.

(v) Recently, many new artificial photosynthesis processes by microorganism/semiconductor composite systems have been developed. The core problem of the artificial photosynthesis system based on microorganisms is the interaction between microorganisms and inorganic materials, the key of which lies in the transfer of energy and charge at the interface. The interface interaction not only affects the expression of microorganisms, but also has an important impact on the properties of materials. Therefore, it is very important to improve the solar energy to chemical energy conversion efficiency of artificial photosynthesis systems based on microorganisms by increasing the interface charge transfer rate.

(vi) Advanced *in-situ* and atomic-scale analysis, and computational simulation techniques will play an important role in EAP. Through advanced *in-situ* micro-analysis and computational simulation, scientists can fully understand the complex reaction process and intermediate products in CO_2/H_2O photoconversion, and thus help overcome the obstacles in energy efficiency, reaction selectivity and total conversion rate.

How to convert CO_2 from human respiration into O_2? How to use CO_2/H_2O on Mars or in other extraterrestrial atmospheric environments to generate O_2 and fuel? These are the core missions of human beings with regard to achieving extraterrestrial survival and sustainable exploration. In recent years, driven by sustainable development on Earth, the technology of artificial photosynthesis has rapidly developed. In space exploration activities, it will become a core ability to *in-situ* transform CO_2/H_2O at room temperature into the basic material needed for human beings to survive outside the Earth. Chinese scientists put forward the concept of EAP, took the lead in developing artificial photosynthesis devices and space experiments that will greatly promote the development of this field, and will guide research in the fields of materials, physics, chemistry, energy, aerospace science and technology.

FUNDING

This work was supported primarily by the National Key Research and Development Program of China (2020YFA0710302 and 2018YFE0208500), the Major Research Plan of the National Natural Science Foundation of China (91963206), the National Natural Science Foundation of China (52072169, 51627810, 51972164 and 51972167), the Program for Guangdong Introducing Innovative and Entrepreneurial Teams (2019ZT08L101), the Natural Science Foundation of Jiangsu Province (SBK2018022120), the open fund of Wuhan National Laboratory for Optoelectronics (2018WNLOKF020), the Postgraduate Research and Practice Innovation Program of Jiangsu Province (KYCX19_0043), the Fundamental Research Funds for the Central Universities (14380180), the Civil Aerospace Technology Research Project (B0108), and the Foshan Xianhu Laboratory of the Advanced Energy Science and Technology Guangdong Laboratory.

Conflict of interest statement. None declared.

REFERENCES

1. Tu W, Zhou Y and Zou Z. Photocatalytic conversion of CO_2 into renewable hydrocarbon fuels: state-of-the-art accomplishment, challenges, and prospects. *Adv Mater* 2014; **26**: 4607–26.

2. Zou ZG, Ye JH and Sayama K *et al.* Direct splitting of water under visible light irradiation with an oxide semiconductor photocatalyst. *Nature* 2001; **414**: 625–7.
3. Kim TW and Choi KS. Nanoporous $BiVO_4$ photoanodes with dual-layer oxygen evolution catalysts for solar water splitting. *Science* 2014; **343**: 990–4.
4. Inoue T, Fujishima A and Konishi S *et al.* Photoelectrocatalytic reduction of carbon dioxide in aqueous suspensions of semiconductor powders. *Nature* 1979; **277**: 637–8.
5. Han H and Li C. Photocatalysis in solar fuel production. *Natl Sci Rev* 2015; **2**: 145–7.
6. Junaedi C, Hawley K and Walsh D *et al.* Compact and lightweight sabatier reactor for carbon dioxide reduction. In: *41st International Conference on Environmental Systems (ICES)*, Portland, OR, USA, 17–21 July 2011.
7. Chevallier F, Feng L and Bösch H *et al.* On the impact of transport model errors for the estimation of CO_2 surface fluxes from GOSAT observations. *Geophys Res Lett* 2010; **37**: L21803.
8. Sakurai M, Oguchi M and Yoshihara S *et al.* Water electrolysis cell that are free liquid-gas separation system for microgravity conditions in order to establish circulated life support system. *J Jpn Soc Microgravity Appl* 2008; **25**: 653–6.
9. Sakurai M, Terao T and Sone Y. Development of water electrolysis system for oxygen production aimed at energy saving and high safety. In: *45th International Conference on Environmental Systems (ICES)*, Bellevue, USA, 12–16 July 2015.
10. Matsushima H, Fukunaka Y and Kuribayashi K. Water electrolysis under microgravity: part II. Description of gas bubble evolution phenomena. *Electrochim Acta* 2006; **51**: 4190–8.
11. Matsushima H, Nishida T and Konishi Y *et al.* Water electrolysis under microgravity: part 1. Experimental technique. *Electrochim Acta* 2003; **48**: 4119–25.
12. Kiuchi D, Matsushima H and Fukunaka Y *et al.* Ohmic resistance measurement of bubble froth layer in water electrolysis under microgravity. *J Electrochem Soc* 2006; **153**: 138–43.
13. Hammarstrom L and Hammes-Schiffer S. Artificial photosynthesis and solar fuels. *Acc Chem Res* 2009; **42**: 1859–60.
14. Feng DQ, Zhang C and Jiang WJ *et al.* Design and trial of extraterrestrial artificial photosynthesis device. *Chinese Space Sci Technol* 2020; **40**: 13–22.
15. Yan SC, Ouyang SX and Gao J *et al.* A room-temperature reactive-template route to mesoporous $ZnGa_2O_4$ with improved photocatalytic activity in reduction of CO_2. *Angew Chem Int Ed* 2010; **49**: 6400–4.
16. Liu C, Colon BC and Ziesack M *et al.* Water splitting-biosynthetic system with CO_2 reduction efficiencies exceeding photosynthesis. *Science* 2016; **352**: 1210–3.
17. Sakimoto KK, Wong AB and Yang PD. Self-photosensitization of nonphotosynthetic bacteria for solar-to-chemical production. *Science* 2016; **351**: 74–7.
18. Su YD, Cestellos-Blanco S and Kim JM *et al.* Close-packed nanowire-bacteria hybrids for efficient solar-driven CO_2 fixation. *Joule* 2020; **4**: 800–11.
19. Tong W, Forster M and Dionigi F *et al.* Electrolysis of low-grade and saline surface water. *Nat Energy* 2020; **5**: 367–77.
20. Samplatsky DJ, Grohs K and Edeen M *et al.* Development and integration of the flight sabatier assembly on the ISS. In: *41st International Conference on Environmental Systems (ICES)*, Portland, OR, USA, 17–21 July 2011.
21. Sakurai M, Oguchi M and Hoshino T *et al.* Water electrolysis cells designed for microgravity conditions in order to establish air revitalization system. In: *35th International Conference on Environmental Systems (ICES)*, Rome, Italy, 11–14 July 2005.
22. Kaplan D, Baird R and Flynn H *et al.* The 2001 Mars *in-situ*-propellant-production precursor (MIP) flight demonstration-project objectives and qualification test results. In: *Space 2000 Conference and Exposition*, Long Beach, USA, 19–21 September 2000.
23. Interbartolo MA, Sanders GB and Oryshchyn L *et al.* Prototype development of an integrated Mars atmosphere and soil-processing system. *J Aerosp Eng* 2013; **26**: 57–66.
24. Hinterman E and Hoffman JA. Simulating oxygen production on Mars for the Mars oxygen in-situ resource utilization experiment. *Acta Astronaut* 2020; **170**: 678–85.
25. NASA Space Science Data Coordinated Archive. *Ice on the Moon: A Summary of Clementine and Lunar Prospector Results.* https://nssdc.gsfc.nasa.gov/planetary/ice/ice_moon.html (10 December 2012, date last accessed).
26. Edmondson K, Joslin D and Fetzer C *et al.* Simulation of the Mars surface solar spectra for optimized performance of triple junction solar cells. In: *19th Space Photovoltaic Research and Technology Conference*, Brookpark, OH, USA, 20–22 September 2005.
27. Rapp D. *Use of Extraterrestrial Resources for Human Space Missions to Moon or Mars.* New York: Springer, 2018.
28. Niles PB, Catling DC and Berger G *et al.* Geochemistry of carbonates on Mars: implications for climate history and nature of aqueous environments. *Space Sci Rev* 2013; **174**: 301–28.
29. Boynton WV, Ming DW and Kounaves SP *et al.* Evidence for calcium carbonate at the Mars Phoenix landing site. *Science* 2009; **325**: 61–4.
30. Fu J, Jiang K and Qiu X *et al.* Product selectivity of photocatalytic CO_2 reduction reactions. *Mater Today* 2020; **32**: 222–43.
31. Wolff CM, Frischmann PD and Schulze M *et al.* All-in-one visible-light-driven water splitting by combining nanoparticulate and molecular co-catalysts on CdS nanorods. *Nat Energy* 2018; **3**: 862–9.
32. Wang J, Lin S and Tian N *et al.* Nanostructured metal sulfides: classification, modification strategy, and solar-driven CO_2 reduction application. *Adv Funct Mater* 2021; **31**: 2008008.
33. Wang Z, Inoue Y and Hisatomi T *et al.* Overall water splitting by Ta_3N_5 nanorod single crystals grown on the edges of $KTaO_3$ particles. *Nat Catal* 2018; **1**: 756–63.
34. Zhang W, Mohamed AR and Ong WJ. Z-scheme photocatalytic systems for carbon dioxide reduction: where are we now? *Angew Chem Int Ed* 2020; **59**: 22894–915.
35. Takata T, Jiang JZ and Sakata Y *et al.* Photocatalytic water splitting with a quantum efficiency of almost unity. *Nature* 2020; **581**: 411–4.
36. Chen LF, Wang Z and Kang P. Efficient photoelectrocatalytic CO_2 reduction by cobalt complexes at silicon electrode. *Chin J Catal* 2018; **39**: 413–20.
37. Zhong Z, Li R and Lin W *et al.* One-dimensional nanocrystals of cobalt perylene diimide polymer with *in-situ* generated FeOOH for efficient photocatalytic water oxidation. *Appl Catal B* 2020; **260**: 118135.
38. Melo MA, Centurion HA and Lucas TTA *et al.* Pseudobrookite Fe_2TiO_5 nanoparticles loaded with earth-abundant nanosized NiO and Co_3O_4 cocatalysts for photocatalytic O_2 evolution via solar water splitting. *ACS Appl Nano Mater* 2020; **3**: 9303–17.
39. Ahmed MG, Zhang MY and Tay YF *et al.* Surface modification of hematite photoanodes with CeO_x cocatalyst for improved photoelectrochemical water oxidation kinetics. *ChemSusChem* 2020; **13**: 5489–96.
40. Zhang GW, Wang B and Li L *et al.* Tailoring the electronic structure by constructing the heterointerface of RuO_2-NiO for overall water splitting with ultralow overpotential and extra-long lifetime. *J Mater Chem A* 2020; **8**: 18945–54.

41. Mine S, Lionet Z and Shigemitsu H *et al.* Design of Fe-MOF-bpdc deposited with cobalt oxide (CoO_x) nanoparticles for enhanced visible-light-promoted water oxidation reaction. *Res Chem Intermed* 2020; **46**: 2003–15.
42. Tian L, Zhai XH and Wang X *et al.* Advances in manganese-based oxides for oxygen evolution reaction. *J Mater Chem A* 2020; **8**: 14400–14.
43. Zeng S, Vahidzadeh E and VanEssen CG *et al.* Optical control of selectivity of high rate CO_2 photoreduction via interband- or hot electron Z-scheme reaction pathways in Au-TiO_2 plasmonic photonic crystal photocatalyst. *Appl Catal B* 2020; **267**: 118644.
44. Ishii T, Anzai A and Yamamoto A *et al.* Calcium zirconate photocatalyst and silver cocatalyst for reduction of carbon dioxide with water. *Appl Catal B* 2020; **277**: 119192.
45. Li Y, Li BH and Zhang DN *et al.* Crystalline carbon nitride supported copper single atoms for photocatalytic CO_2 reduction with nearly 100% CO selectivity. *ACS Nano* 2020; **14**: 10552–61.
46. Yang J, Wang ZY and Jiang JC *et al. In-situ* polymerization induced atomically dispersed manganese sites as cocatalyst for CO_2 photoreduction into synthesis gas. *Nano Energy* 2020; **76**: 105059.
47. Li K, Lin YZ and Wang K *et al.* Rational design of cocatalyst system for improving the photocatalytic hydrogen evolution activity of graphite carbon nitride. *Appl Catal B* 2020; **268**: 118402.
48. Jian QY, Hao XQ and Jin ZL *et al.* Amorphous tungsten phosphosulphide-modified CdS nanorods as a highly efficient electron-cocatalyst for enhanced photocatalytic hydrogen production. *Phys Chem Chem Phys* 2020; **22**: 1932–43.
49. Lee I, Kim WJ and Lee DC. Design of metallic cocatalysts in heterostructured nanoparticles for photocatalytic CO_2-to-hydrocarbon conversion. *J Phys D: Appl Phys* 2020; **53**: 123001.
50. Li P, Liu L and An W *et al.* Ultrathin porous *g*—C_3N_4 nanosheets modified with AuCu alloy nanoparticles and C–C coupling photothermal catalytic reduction of CO_2 to ethanol. *Appl Catal B* 2020; **266**: 118618.
51. Ran J, Jaroniec M and Qiao SZ. Cocatalysts in semiconductor-based photocatalytic CO_2 reduction: achievements, challenges, and opportunities. *Adv Mater* 2018; **30**: 1704649.
52. Yan SC, Wang JJ and Gao HL *et al.* Zinc gallogermanate solid solution: a novel photocatalyst for efficiently converting CO_2 into solar fuels. *Adv Funct Mater* 2013; **23**: 1839–45.
53. Maeda K, Teramura K and Lu DL *et al.* Photocatalyst releasing hydrogen from water. *Nature* 2006; **440**: 295.
54. Li P, Zhou Y and Zhao Z *et al.* Hexahedron prism-anchored octahedronal CeO_2: crystal facet-based homojunction promoting efficient solar fuel synthesis. *J Am Chem Soc* 2015; **137**: 9547–50.
55. Zhou P, Wang X and Yan SC *et al.* Solid solution photocatalyst with spontaneous polarization exhibiting low recombination toward efficient CO_2 photoreduction. *ChemSusChem* 2016; **9**: 2064–8.
56. Li Z, Zhang L and Liu Y *et al.* Surface polarity-induced spatial charge separation boosts photocatalytic overall water splitting on GaN nanorod arrays. *Angew Chem Int Ed* 2020; **59**: 935–42.
57. Wang Y, Liu X and Han X *et al.* Unique hole-accepting carbon-dots promoting selective carbon dioxide reduction nearly 100% to methanol by pure water. *Nat Commun* 2020; **11**: 2531.
58. Wang Q, Warnan J and Rodríguez-Jiménez S *et al.* Molecularly engineered photocatalyst sheet for scalable solar formate production from carbon dioxide and water. *Nat Energy* 2020; **5**: 703–10.
59. Wang Y, Zhang ZZ and Zhang LN *et al.* Visible-light driven overall conversion of CO_2 and H_2O to CH_4 and O_2 on 3D-SiC@2D-MoS_2 heterostructure. *J Am Chem Soc* 2018; **140**: 14595–8.
60. Dong LZ, Zhang L and Liu J *et al.* Stable heterometallic cluster-based organic framework catalysts for artificial photosynthesis. *Angew Chem Int Ed* 2020; **59**: 2659–63.
61. Okazaki M, Suganami Y and Hirayama N *et al.* Site-selective deposition of a cobalt cocatalyst onto a plasmonic Au/TiO_2 photoanode for improved water oxidation. *ACS Appl Energy Mater* 2020; **3**: 5142–6.
62. Zhang N, Wang X and Feng J *et al.* Paving the road toward the use of β-Fe_2O_3 in solar water splitting: Raman identification, phase transformation and strategies for phase stabilization. *Natl Sci Rev* 2020; **7**: 1059–67.
63. Shao C, Malik AS and Han J *et al.* Oxygen vacancy engineering with flame heating approach towards enhanced photoelectrochemical water oxidation on WO_3 photoanode. *Nano Energy* 2020; **77**: 105190.
64. Lim FS, Tan ST and Zhu Y *et al.* Tunable plasmon-induced charge transport and photon absorption of bimetallic Au–Ag nanoparticles on ZnO photoanode for photoelectrochemical enhancement under visible light. *J Phys Chem C* 2020; **124**: 14105–17.
65. Xiao Y, Feng C and Fu J *et al.* Band structure engineering and defect control of Ta_3N_5 for efficient photoelectrochemical water oxidation. *Nat Catal* 2020; **3**: 932–40.
66. Oh K, Dorcet V and Fabre B *et al.* Dissociating water at n-Si photoanodes partially covered with Fe catalysts. *Adv Energy Mater* 2020; **10**: 1902963.
67. Thalluri SM, Wei B and Welter K *et al.* Inverted pyramid textured p-silicon covered with Co_2P as an efficient and stable solar hydrogen evolution photocathode. *ACS Energy Lett* 2019; **4**: 1755–62.
68. Matsumoto Y, Sugiyama K and Sato E. New photocathode materials for hydrogen evolution: calcium iron oxide ($CaFe_2O_4$) and strontium iron oxide ($Sr_7Fe_{10}O_{22}$). *J Phys Chem* 1987; **91**: 577–81.
69. Viswanathan B, Subramanian VR and Lee JS. *Materials and Processes for Solar Fuel Production.* New York: Springer, 2014.
70. Prévot MS, Guijarro N and Sivula K. Enhancing the performance of a robust sol–gel-processed p-type delafossite $CuFeO_2$ photocathode for solar water reduction. *ChemSusChem* 2015; **8**: 1359–67.
71. Joshi UA and Maggard PA. $CuNb_3O_8$: a p-type semiconducting metal oxide photoelectrode. *J Phys Chem C* 2012; **3**: 1577–81.
72. Liu Z, Zhao Z-G and Miyauchi M. Efficient visible light active $CaFe_2O_4$/WO_3 based composite photocatalysts: effect of interfacial modification. *J Phys Chem C* 2009; **113**: 17132–7.
73. Nian J-N, Hu C-C and Teng H. Electrodeposited p-type Cu_2O for H_2 evolution from photoelectrolysis of water under visible light illumination. *Int J Hydrogen Energy* 2008; **33**: 2897–903.
74. Feng K, Huang D and Li L *et al.* MoS_x-CdS/Cu_2ZnSnS_4-based thin film photocathode for solar hydrogen evolution from water. *Appl Catal B* 2020; **268**: 118438.
75. Kuehnel MF, Creissen CE and Sahm CD *et al.* ZnSe nanorods as visible-light absorbers for photocatalytic and photoelectrochemical H_2 evolution in water. *Angew Chem Int Ed* 2019; **58**: 5059–63.
76. Wang QL, Wang XK and Yu ZH *et al.* Artificial photosynthesis of ethanol using type-II *g*-C_3N_4/ZnTe heterojunction in photoelectrochemical CO_2 reduction system. *Nano Energy* 2019; **60**: 827–35.
77. Chang X, Wang T and Yang P *et al.* The development of cocatalysts for photoelectrochemical CO_2 reduction. *Adv Mater* 2019; **31**: 1804710.

78. Zhang N, Long R and Gao C *et al.* Recent progress on advanced design for photoelectrochemical reduction of CO_2 to fuels. *Sci China Mater* 2018; **61**: 771–805.
79. Maier CU, Specht M and Bilger G. Hydrogen evolution on platinum-coated p-silicon photocathodes. *Int J Hydrogen Energy* 1996; **21**: 859–64.
80. Feng J, Gong M and Kenney MJ *et al.* Nickel-coated silicon photocathode for water splitting in alkaline electrolytes. *Nano Res* 2015; **8**: 1577–83.
81. Benck JD, Lee SC and Fong KD *et al.* Designing active and stable silicon photocathodes for solar hydrogen production using molybdenum sulfide nanomaterials. *Adv Energy Mater* 2014; **4**: 1400739.
82. Zhong X, Wang G and Papandrea B *et al.* Reduced graphene oxide/silicon nanowire heterostructures with enhanced photoactivity and superior photoelectrochemical stability. *Nano Res* 2015; **8**: 2850–8.
83. Kargar A, Cheung JS and Liu C-H *et al.* NiO_x-Fe_2O_3-coated p-Si photocathodes for enhanced solar water splitting in neutral pH water. *Nanoscale* 2015; **7**: 4900–5.
84. Choi MJ, Jung J-Y and Park M-J *et al.* Long-term durable silicon photocathode protected by a thin Al_2O_3/SiO_x layer for photoelectrochemical hydrogen evolution. *J Mater Chem A* 2014; **2**: 2928–33.
85. Stelzner T, Pietsch M and Andrä G *et al.* Silicon nanowire-based solar cells. *Nanotechnology* 2008; **19**: 295203.
86. Hou Y, Abrams BL and Vesborg PCK *et al.* Bioinspired molecular co-catalysts bonded to a silicon photocathode for solar hydrogen evolution. *Nat Mater* 2011; **10**: 434–8.
87. Chen CJ, Yang KC and Liu CW *et al.* Silicon microwire arrays decorated with amorphous heterometal-doped molybdenum sulfide for water photoelectrolysis. *Nano Energy* 2017; **32**: 422–32.
88. Zhang H, Ding Q and He D *et al.* A p-Si/$NiCoSe_x$ core/shell nanopillar array photocathode for enhanced photoelectrochemical hydrogen production. *Energy Environ Sci* 2016; **9**: 3113–9.
89. Morales-Guio CG, Thorwarth K and Niesen B *et al.* Solar hydrogen production by amorphous silicon photocathodes coated with a magnetron sputter deposited Mo_2C catalyst. *J Am Chem Soc* 2015; **137**: 7035–8.
90. Gurudayal, Beeman JW and Bullock J *et al.* Si photocathode with Ag-supported dendritic Cu catalyst for CO_2 reduction. *Energy Environ Sci* 2019; **12**: 1068–77.
91. Lin CY, Lai YH and Mersch D *et al.* $Cu_2O|NiO_x$ nanocomposite as an inexpensive photocathode in photoelectrochemical water splitting. *Chem Sci* 2012; **3**: 3482–7.
92. Yang C, Tran PD and Boix PP *et al.* Engineering a $Cu_2O/NiO/Cu_2MoS_4$ hybrid photocathode for H_2 generation in water. *Nanoscale* 2014; **6**: 6506–10.
93. Yang Y, Xu D and Wu Q *et al.* Cu_2O/CuO bilayered composite as a high-efficiency photocathode for photoelectrochemical hydrogen evolution reaction. *Sci Rep* 2016; **6**: 35158.
94. Stepek IA, Cao T and Koetemann A *et al.* Antibiotic discovery with synthetic fermentation: library assembly, phenotypic screening, and mechanism of action of beta-peptides targeting penicillin-binding proteins. *ACS Chem Biol* 2019; **14**: 1030–40.
95. Morales-Guio CG, Tilley SD and Vrubel H *et al.* Hydrogen evolution from a copper(I) oxide photocathode coated with an amorphous molybdenum sulphide catalyst. *Nat Commun* 2014; **5**: 3059.
96. Paracchino A, Laporte V and Sivula K *et al.* Highly active oxide photocathode for photoelectrochemical water reduction. *Nat Mater* 2011; **10**: 456–61.
97. Pan L, Liu Y and Yao L *et al.* Cu_2O photocathodes with band-tail states assisted hole transport for standalone solar water splitting. *Nat Commun* 2020; **11**: 318.
98. DuChene JS, Tagliabue G and Welch AJ *et al.* Optical excitation of a nanoparticle Cu/p-NiO photocathode improves reaction selectivity for CO_2 reduction in aqueous electrolytes. *Nano Lett* 2020; **20**: 2348–58.
99. Zhang L, Minegishi T and Kubota J *et al.* Hydrogen evolution from water using $AgxCu_{1-x}GaSe_2$ photocathodes under visible light. *Phys Chem Chem Phys* 2014; **16**: 6167–74.
100. Yang W, Kim JH and Hutter OS *et al.* Benchmark performance of low-cost Sb_2Se_3 photocathodes for unassisted solar overall water splitting. *Nat Commun* 2020; **11**: 861.
101. Zhou BW, Ou PF and Pant N *et al.* Highly efficient binary copper-iron catalyst for photoelectrochemical carbon dioxide reduction toward methane. *Proc Natl Acad Sci USA* 2020; **117**: 1330–8.
102. Li H, Wen P and Itanze DS *et al.* Colloidal silver diphosphide (AgP_2) nanocrystals as low overpotential catalysts for CO_2 reduction to tunable syngas. *Nat Commun* 2019; **10**: 5724.
103. Wang RY, Liu HD and Fan ZW *et al.* Unconventional gas-based bottom-up, meter-area-scale fabrication of hydrogen-bond free *g*-CN nanorod arrays and coupling layers with TiO_2 toward high-efficiency photoelectrochemical performance. *Nanoscale* 2018; **10**: 3342–9.
104. Liao AZ, Chen RT and Fan FT *et al.* Integration of Fe_xS electrocatalysts and simultaneously generated interfacial oxygen vacancies to synergistically boost photoelectrochemical water splitting of Fe_2O_3 photoanodes. *Chem Commun* 2018; **54**: 13817–20.
105. Song ZM, Zhu XD and Zeng YS *et al.* Cobalt phosphate cocatalyst loaded-CdS nanorod photoanode with well-defined junctions for highly efficient photoelectrochemical water splitting. *Catal Lett* 2020; **150**: 1878–89.
106. Chong RF, Du YQ and Chang ZX *et al.* 2D co-incorporated hydroxyapatite nanoarchitecture as a potential efficient oxygen evolution cocatalyst for boosting photoelectrochemical water splitting on Fe_2O_3 photoanode. *Appl Catal B* 2019; **250**: 224–33.
107. Bedin KC, Muche DNF and Melo MA *et al.* Role of cocatalysts on hematite photoanodes in photoelectrocatalytic water splitting: challenges and future perspectives. *ChemCatChem* 2020; **12**: 3156–69.
108. Zhu H, Zhao MM and Zhou JK *et al.* Surface states as electron transfer pathway enhanced charge separation in TiO2 nanotube water splitting photoanodes. *Appl Catal B* 2018; **234**: 100–8.
109. Wang S, He T and Chen P *et al. In situ* formation of oxygen vacancies achieving near-complete charge separation in planar $BiVO_4$ photoanodes. *Adv Mater* 2020; **32**: 2001385.
110. Zhang BB, Wang L and Zhang YJ *et al.* Ultrathin FeOOH nanolayers with abundant oxygen vacancies on $BiVO_4$ photoanodes for efficient water oxidation. *Angew Chem Int Ed* 2018; **57**: 2248–52.
111. Zhang B, Huang X and Zhang Y *et al.* Unveiling the activity and stability origin of $BiVO_4$ photoanodes with FeNi oxyhydroxides for oxygen evolution. *Angew Chem Int Ed* 2020; **59**: 18990–5.
112. Zhang K, Jin B and Park C *et al.* Black phosphorene as a hole extraction layer boosting solar water splitting of oxygen evolution catalysts. *Nat Commun* 2019; **10**: 2001.
113. Hu YF, Wu YQ and Feng JY *et al.* Rational design of electrocatalysts for simultaneously promoting bulk charge separation and surface charge transfer in solar water splitting photoelectrodes. *J Mater Chem A* 2018; **6**: 2568–76.
114. He J and Janaky C. Recent advances in solar-driven carbon dioxide conversion: expectations versus reality. *ACS Energy Lett* 2020; **5**: 1996–2014.
115. Schreier M, Curvat L and Giordano F *et al.* Efficient photosynthesis of carbon monoxide from CO_2 using perovskite photovoltaics. *Nat Commun* 2015; **6**: 7326.

116. Wang Y, Liu J and Wang Y *et al*. Efficient solar-driven electrocatalytic CO_2 reduction in a redox-medium-assisted system. *Nat Commun* 2018; **9**: 5003.
117. Nath NCD, Choi SY and Jeong HW *et al*. Stand-alone photoconversion of carbon dioxide on copper oxide wire arrays powered by tungsten trioxide/dye-sensitized solar cell dual absorbers. *Nano Energy* 2016; **25**: 51–9.
118. Huan TN, Corte DAD and Lamaison S *et al*. Low-cost high-efficiency system for solar-driven conversion of CO_2 to hydrocarbons. *Proc Natl Acad Sci USA* 2019; **116**: 9735–40.
119. Mi Y, Qiu Y and Liu Y *et al*. Cobalt—iron oxide nanosheets for high-efficiency solar-driven CO_2-H_2O coupling electrocatalytic reactions. *Adv Funct Mater* 2020; **30**: 2003438.
120. Kuk SK, Ham Y and Gopinath K *et al*. Continuous 3D titanium nitride nanoshell structure for solar-driven unbiased biocatalytic CO_2 reduction. *Adv Energy Mater* 2019; **9**: 1900029.
121. Shen Z, Xia Y and Yang Y *et al*. Protection of materials and structures from space radiation environments on spacecraft. *Aerosp Mater Technol* 2020; **50**: 1–7.